

Black Hole Solutions in Non-Minimally Coupled Weyl Connection Gravity

M. Margarida Lima ^{1,2,3} and Cláudio Gomes ^{3,4,*}

¹ Departamento de Física, Instituto Superior Técnico, Universidade de Lisboa, Av. Rovisco Pais, 1049-001 Lisboa, Portugal; margarida.a.lima@tecnico.ulisboa.pt

² Centro de Análise Matemática, Geometria e Sistemas Dinâmicos, Instituto Superior Técnico, Universidade de Lisboa, Av. Rovisco Pais, 1049-001 Lisboa, Portugal

³ OKEANOS–Instituto de Investigação em Ciências do Mar, Universidade dos Açores, Rua Prof. Doutor Frederico Machado, 4, 9901-862 Horta, Portugal

⁴ Centro de Física das Universidades do Minho e do Porto, Rua do Campo Alegre s/n, 4169-007 Porto, Portugal

*Corresponding author: Cláudio Gomes; claudio.fv.gomes@uac.pt

Abstract

Schwarzschild and Reissner–Nordstrøm black hole solutions are found in the context of a non-minimal matter–curvature coupling with Weyl connection both in vacuum and in the presence of a cosmological constant-like matter content. This model has the advantage of an extra force term which can mimic dark matter and dark energy, and simultaneously following Weyl’s idea of unifying gravity and electromagnetism. In fact, vacuum Schwarzschild solutions differ from the ones in a constant curvature scenario in $f(R)$ theories, with the appearance of a coefficient in the term that is linear in r and a corrected “cosmological constant”. Non-vacuum Schwarzschild solutions formally have the same solutions as in the previous case, with the exception being the physical interpretation of a cosmological constant as the source of the matter Lagrangian and not a simple reparameterization of the $f(R)$ description. Reissner–Nordstrøm solutions cannot be found in a vacuum, only in the presence of matter fields, with the result that the solutions also differ from the constant curvature scenario in $f(R)$ theories by the term being linear in r , the corrected/dressed charge, and the cosmological constant. These results have bearings on future numerical simulations for black holes and gravitational waves in next-generation wavelet templates.

Keywords: black holes; Schwarzschild; Reissner–Nordstrøm; Weyl connection gravity; non-minimal coupling; modified gravity; $f(R)$ theory

1 Introduction

General relativity is one of the mathematically simplest theories of gravity that obey several physical and observational requirements. However, there are some problems on both small and large scales. At small scales, it is not compatible with quantum mechanics; hence, we still do not have a complete theory of gravity in the so-called UV regime. At the large scale, both dark matter and dark energy are required in order to account for the data; however, we still do not exactly know what they are made of. Additionally, there are the well-known problems of the cosmological constant and the existence of singularities. Therefore, several alternative models to Einstein's theory have been proposed to account for astrophysical and cosmological data (see, e.g., [1, 2, 3]).

One of the most famous extensions of general relativity consists of the so-called $f(R)$ theories [4, 5]. A further extension includes a non-minimal coupling between matter and curvature [6], which leads to a non-conservation law for the energy–momentum tensor built from matter fields. This feature allows for mimicking dark matter and dark energy [7, 8, 9]. Furthermore, this model has been explored in several astrophysical and cosmological contexts [10, 11, 12, 13, 14, 15, 16, 17, 18, 19, 20, 21].

Usually, these approaches are based on a symmetric connection that is metric compatible, $\nabla_{\mu}g^{\mu\nu} = 0$. Nevertheless, there are other promising avenues, such as when looking into torsion T and non-metricity Q . In fact, it is possible to formulate three gravity models that are equivalent to each other in general relativity where the gravity field is either the metric, the torsion, or related to the non-metricity. This is not the case in theories that deviate from Einstein's theory [22]. Likewise, for the $f(R)$ extension of general relativity, we can have $f(T)$ [23] and $f(Q)$ [24, 25].

As expected, the non-minimal matter–curvature coupling model has been extended to its non-metricity version [26], where the scalar curvature is replaced by the scalar non-metricity. Another realization involves considering that the geometry is not described by the metric field alone but also by a vector field which is related to the metric field via the non-metricity property, namely, $D_{\mu}g^{\mu\nu} = A_{\mu}g^{\mu\nu}$. This is called the Weyl connection gravity, and is not necessarily the same as the so-called Weyl gravity, where there is a squared Weyl tensor in the action functional. Recall that this was Weyl's attempt to incorporate electromagnetism into general relativity via non-metricity, similar to the Kaluza–Klein model with an extra fifth dimension [27, 28], despite criticisms from Einstein given the possibility of continuous and arbitrary length variation of a vector from one point to another in space–time (except, e.g., for a charge particle, the Weyl vector is purely imaginary, and, hence, problematic). Moreover, as far as matter fields are concerned, it has been shown that local scale invariance leads to the existence of a Weyl vector meson that absorbs the Higgs particle remaining in the Weinberg–Salam model [29]. This Weyl vector meson, coined the metron, may interact with spinor fields under certain conditions [30]. Moreover, the sources of a general non-metricity have been shown to be the shear and dilation currents, which also couple to the former [31].

The Weyl connection realization has been generalized into a non-minimal version [32]. This model has proven to also admit cosmological solutions when the Weyl vector is dynamical and identified as a gauge vector [33]. In the latter scenario, it can be safe from Ostrogradsky instabilities (which arise in non-degenerate Lagrangian densities of theories that have higher order derivatives with respect to time, leading to unbounded states of energy) if either the extrinsic curvature scalar of the hypersurface of the space–time foliation is zero or if the Weyl vector has only spatial components [34].

A further analysis of gravity models concerns black hole solutions and their stability. In fact, analytic solutions in theories beyond general relativity are not trivial, and in many cases some assumptions or simplifications are required. Thus, black hole solutions have been found by assuming constant curvature, by using perturbative methods in $f(R)$ theories [35, 36, 37, 38, 39],

in the non-minimal matter–curvature coupling gravity model imposing the Newtonian limit (as in general relativity [40] and Weyl gravity built from the Weyl tensor [41]), or even by looking into quasinormal modes in the latter model [42]. Moreover, it is also possible to study the thermodynamics of black hole solutions [43] in modified gravity [44, 45, 46, 47, 48, 49].

Thus, in this manuscript, we aim to find black hole solutions in the context of non-minimally coupled Weyl connection gravity.

The rest of this paper is organized as follows. In Section 2, we present the model and some of its properties. In the next section, we find the Schwarzschild black hole solutions both in a vacuum and assuming matter contribution in the form of a cosmological constant. In Section 4, we study Reissner–Nordström-like solutions in these theories. Finally, we draw our conclusions in Section 5.

2 Non-Minimal Matter–Curvature Coupling with Weyl Connection

The Weyl connection gravity model introduces a vector field which provides the non-metricity properties. This model is characterized by the action of the covariant derivative of the metric field tensor not vanishing and being given by

$$D_\lambda g_{\mu\nu} = A_\lambda g_{\mu\nu}, \quad (1)$$

where A_λ is the Weyl vector field, $g_{\mu\nu}$ is the metric tensor, and the generalized covariant derivative is

$$D_\lambda g_{\mu\nu} = \nabla_\lambda g_{\mu\nu} - \bar{\Gamma}_{\mu\lambda}^\rho g_{\rho\nu} - \bar{\Gamma}_{\nu\lambda}^\rho g_{\rho\mu}, \quad (2)$$

where ∇_λ is the usual covariant derivative with Levi–Civita connection, and $\bar{\Gamma}_{\mu\nu}^\rho = -\frac{1}{2}\delta_\nu^\rho A_\mu - \frac{1}{2}\delta_\mu^\rho A_\nu + \frac{1}{2}g_{\mu\nu}A^\rho$ is the disformation tensor which reflects the Weyl non-metricity. Note that in contrast to the Levi–Civita part, which is not tensorial, the disformation piece of the affine connection behaves as a tensor.

The Riemann tensor can be generalized in order to take the Weyl connection into account, $\bar{\Gamma}_{\mu\nu}^\rho = \Gamma_{\mu\nu}^\rho + \bar{\Gamma}_{\mu\nu}^\rho$, such that

$$\bar{R}_{\mu\sigma\nu}^\rho = \partial_\sigma \bar{\Gamma}_{\nu\mu}^\rho - \partial_\nu \bar{\Gamma}_{\sigma\mu}^\rho + \bar{\Gamma}_{\sigma\lambda}^\rho \bar{\Gamma}_{\nu\mu}^\lambda - \bar{\Gamma}_{\nu\lambda}^\rho \bar{\Gamma}_{\sigma\mu}^\lambda. \quad (3)$$

By contracting the first and third indices of this generalized curvature tensor, we introduce the generalized Ricci tensor, which is given by

$$\bar{R}_{\mu\nu} = R_{\mu\nu} + \frac{1}{2}A_\mu A_\nu + \frac{1}{2}g_{\mu\nu}(\nabla_\lambda - A_\lambda)A^\lambda + \tilde{F}_{\mu\nu} + \frac{1}{2}(\nabla_\mu A_\nu + \nabla_\nu A_\mu) = R_{\mu\nu} + \bar{\bar{R}}_{\mu\nu}, \quad (4)$$

where $R_{\mu\nu}$ is the usual Ricci tensor and $\tilde{F}_{\mu\nu} = \partial_\mu A_\nu - \partial_\nu A_\mu = \nabla_\mu A_\nu - \nabla_\nu A_\mu$ is the strength tensor of the Weyl field. It is also easy to see that the trace of the generalized Ricci tensor, that is the scalar curvature with Weyl connection, is given by

$$\bar{R} = R + 3\nabla_\lambda A^\lambda - \frac{3}{2}A_\lambda A^\lambda = R + \bar{\bar{R}}, \quad (5)$$

where R is the usual Ricci curvature.

It is known that the length norm is given by $L^2 = g_{\mu\nu}dx^\mu dx^\nu$. Deriving this expression and applying the relation (2), it turns out that $dL = \frac{1}{2}LA_\lambda dx^\lambda$. This leads to $L = L_0 e^{\frac{1}{2}\int A_\lambda dx^\lambda}$, so the length of a vector may change from one point to another in space–time. As $dL \geq 0$, we should impose the following constraint for the Weyl vector:

$$A_\lambda dx^\lambda \geq 0. \quad (6)$$

These quantities can be used to generalize the non-minimal matter–curvature coupling model [6], to incorporate the Weyl connection, whose action functional takes the form [32]:

$$S = \int (\kappa f_1(\bar{R}) + f_2(\bar{R})\mathcal{L}) \sqrt{-g} d^4x, \quad (7)$$

where $f_1(\bar{R})$ and $f_2(\bar{R})$ are generic functions of the generalized scalar curvature, $\kappa = \frac{1}{16\pi G}$ with G being the Newton’s constant, \mathcal{L} is the matter Lagrangian density, and g is the determinant of the metric field. Throughout this article, we shall consider units such that $\kappa = 1$ without loss of generality.

Varying the action with respect to the vector field, up to boundary terms, we obtain constraint-like equations [32]:

$$\nabla_\lambda \Theta(\bar{R}) = -A_\lambda \Theta(\bar{R}), \quad (8)$$

where $\Theta(\bar{R}) = F_1(\bar{R}) + F_2(\bar{R})\mathcal{L}$ and $F_i(\bar{R}) = \frac{df_i(\bar{R})}{d\bar{R}}$, $i \in \{1, 2\}$.

In its turn, varying the action with respect to the metric, and taking into account the previous equation, we obtain the field equations [32]:

$$\left(R_{\mu\nu} + \bar{\bar{R}}_{(\mu\nu)} \right) \Theta(\bar{R}) - \frac{1}{2} g_{\mu\nu} f_1(\bar{R}) = \frac{f_2(\bar{R})}{2} T_{\mu\nu}, \quad (9)$$

where $\bar{\bar{R}}_{(\mu\nu)} = \frac{1}{2} A_\mu A_\nu + \frac{1}{2} g_{\mu\nu} (\nabla_\lambda - A_\lambda) A^\lambda + \nabla_{(\mu} A_{\nu)}$ and $T_{\mu\nu}$ is the energy-momentum tensor built from the matter Lagrangian, $T_{\mu\nu} = -\frac{2}{\sqrt{-g}} \frac{\delta(\sqrt{-g}\mathcal{L})}{\delta g^{\mu\nu}}$.

The trace of the metric field equations is

$$\Theta(\bar{R})\bar{R} - 2f_1(\bar{R}) = \frac{f_2(\bar{R})}{2} T, \quad (10)$$

where $T = g^{\mu\nu} T_{\mu\nu}$.

Taking the previous relations and plugging them into Equation (9), one obtains the trace-free equations:

$$\Theta(\bar{R}) \left[R_{\mu\nu} - \frac{1}{4} g_{\mu\nu} \bar{R} \right] + \Theta(\bar{R}) \left[\bar{\bar{R}}_{(\mu\nu)} - \frac{1}{4} g_{\mu\nu} \bar{\bar{R}} \right] = \frac{f_2(\bar{R})}{2} \left[T_{\mu\nu} - \frac{1}{4} g_{\mu\nu} T \right]. \quad (11)$$

Note that the constraint Equation (8) reduces the fourth-order theory of the usual non-minimal coupling theory into a second-order version, as we can see in Equation (9). This has the advantage of avoiding ghost instabilities, as it has been demonstrated in Ref. [34], provided that some conditions are met.

Taking the divergence of the field equations, it is possible to obtain the covariant non-conservation law of the energy-momentum tensor [32]:

$$\nabla_\mu T^{\mu\nu} = \frac{2}{f_2(\bar{R})} \left[\frac{F_2(\bar{R})}{2} (g^{\mu\nu} \mathcal{L} - T^{\mu\nu}) \nabla_\mu \bar{R} + \nabla_\mu (\Theta(\bar{R}) B^{\mu\nu}) - \frac{1}{2} (F_1(\bar{R}) g^{\mu\nu} + F_2(\bar{R}) T^{\mu\nu}) \nabla_\mu \bar{\bar{R}} \right], \quad (12)$$

where $B^{\mu\nu} = \frac{3}{2} A^\mu A^\nu + \frac{3}{2} g^{\mu\nu} (\nabla_\lambda - A_\lambda) A^\lambda$. Thus, not only the non-minimal coupling between curvature and matter but also the non-metricity property lead to a non-trivial exchange of energy and momentum between the geometry and matter sectors.

2.1 Geodesic Motion

In order to assess the geodesics in these theories, we consider the energy-momentum tensor for a perfect fluid,

$$T_{\mu\nu} = (\rho + p) u_\mu u_\nu + p g_{\mu\nu}, \quad (13)$$

where ρ is the energy density and p is the pressure. The four-velocity, u_μ , satisfies the conditions $u_\mu u^\mu = -1$ and $u^\mu \nabla_\nu u_\mu = 0$. We also introduce the projection operator $h_{\mu\nu} = g_{\mu\nu} + u_\mu u_\nu$, such that $h_{\mu\nu} u^\mu = 0$.

Contracting Equation (12) with the projection operator $h_{\lambda\nu}$, we obtain

$$(\rho + p)g_{\lambda\nu}u^\mu \nabla_\mu u^\nu + (\nabla_\mu p)(\delta_\lambda^\mu + u_\lambda u^\mu) = \frac{1}{f_2(\bar{R})} \left[(F_2(\bar{R})(\mathcal{L} - p)\nabla_\mu R - (F_1(\bar{R}) + pF_2(\bar{R}))\nabla_\mu \bar{R}) + (\delta_\lambda^\mu + u_\lambda u^\mu) + 2(\nabla_\mu (\Theta(\bar{R})B_\lambda^\mu) - u_\lambda u_\mu \nabla_\mu (\Theta(\bar{R})B^{\mu\nu})) \right]. \quad (14)$$

Finally, contracting the previous relation with $g^{\sigma\lambda}$ leads to the equation of motion for a fluid element:

$$\frac{du^\sigma}{ds} + \Gamma_{\mu\nu}^\sigma u^\mu u^\nu = f^\sigma, \quad (15)$$

where the extra force term reads as follows:

$$f^\sigma = \frac{1}{(\rho + p)} \left[\frac{F_2(\bar{R})}{f_2(\bar{R})} (\mathcal{L} - p)\nabla_\mu R - \nabla_\mu p - \frac{F_1(\bar{R}) + pF_2(\bar{R})}{f_2(\bar{R})} \nabla_\mu \bar{R} + \frac{2\nabla_\nu (\Theta(\bar{R})B_\mu^\nu)}{f_2(\bar{R})} \right] h^{\mu\sigma}. \quad (16)$$

It is straightforward to check that the extra force f^σ is orthogonal to the four-velocity of the particle, $f^\sigma u_\sigma = 0$, due to the properties of the projection operator. Moreover, the first term inside brackets arises from the non-minimal coupling and breaks the degeneracy in the Lagrangian density choice for perfect fluids that happened in general relativity [50, 51]. The second term is the same that stems from general relativity, whilst the last two terms arise from the existence of the non-metricity. In the non-minimal matter–curvature coupling model, the choice of $\mathcal{L} = p$ leads to a vanishing of the extra-force term in the geodesics, while in this model, a vanishing force would also require that $2\nabla_\nu (\Theta(\bar{R})B_\mu^\nu) - (F_1(\bar{R}) + pF_2(\bar{R}))\nabla_\mu \bar{R} = 0$ for that choice.

2.2 Maxwell Equations

The presence of this non-minimal coupling implies that the physical implications of gravity over matter fields can be quite different from one type to another. In particular, charged matter fields have modified dynamics. Let us consider the electromagnetic Lagrangian density

$$\mathcal{L}^{(EM)} = -\frac{1}{4}F_{\mu\nu}F^{\mu\nu}, \quad (17)$$

where $F_{\mu\nu} = \partial_\mu \Phi_\nu - \partial_\nu \Phi_\mu$ is the Faraday tensor and Φ_μ is the electromagnetic four-potential.

The energy momentum tensor of the electromagnetic field is given by

$$T_{\mu\nu}^{(EM)} = F_{\mu\alpha}F_\nu^\alpha - \frac{1}{4}g_{\mu\nu}F_{\alpha\beta}F^{\alpha\beta}. \quad (18)$$

When this Lagrangian is considered in the action (7), the variation with respect to the four-potential leads to the inhomogeneous modified Maxwell equations

$$\nabla_\mu (f_2(\bar{R})F^{\mu\nu}) = 0. \quad (19)$$

As we shall see in Section 4, these modifications will be important when analyzing the black hole solutions with electric charge.

2.3 Static Spherically Symmetric Ansatz

In order to obtain the black hole solutions of the non-minimally coupled Weyl connection gravity model, we consider the static line element in spherical coordinates:

$$ds^2 = -e^{\alpha(r)}dt^2 + e^{\beta(r)}dr^2 + r^2(d\theta^2 + \sin^2(\theta)d\phi^2), \quad (20)$$

where $\alpha(r)$ and $\beta(r)$ are arbitrary functions of the distance, r .

Since non-rotating black holes are static spherically symmetric solutions of a gravity theory, the vector Weyl field should not change with time. Furthermore, we do not expect this to break isotropy so its components only depend on the distance. Thus, the vector takes the form $A_\mu = (A_0(r), A_1(r), A_2(r), A_3(r))$, where $A_i(r)$, with $i \in \{0, 1, 2, 3\}$, are arbitrary functions of the distance.

Throughout this work, we seek to find and analyze solutions in a vacuum and in the presence of a ‘‘cosmological constant’’-like matter. Hence, in both cases, the field Equation (9) implies that $\bar{R}_{(\mu\nu)} = 0$, when $\mu \neq \nu$. These relations can be converted to constraints to the Weyl vector, A_μ .

After some calculations, it is possible to conclude that there exist two types of vectors: $A_\mu = (A_0(r), A_1(r), 0, 0)$, such that $A'_0(r) + (A_1(r) - \alpha'(r))A_0(r) = 0$; and $A_\mu = (0, A_1(r), A_2(r), 0)$, such that $A'_2(r) + (A_1(r) - \frac{2}{r})A_2(r) = 0$, where the prime, $'$, denotes the derivative in order to r . However, it is possible to see that, in the second case, the field equations imply that $A_2(r) = 0$. Thus, considering the static configuration of the problem, the Weyl vector can only take one of the following forms:

$$A_\mu = (0, A(r), 0, 0), \quad (21a)$$

$$A_\mu = (A_0(r), A_1(r), 0, 0), \text{ with } A_0(r) \neq 0 \text{ and } A'_0(r) + (A_1(r) - \alpha'(r))A_0(r) = 0. \quad (21b)$$

Taking into account the constraint (6), the previous vectors must satisfy, respectively, the following conditions:

$$A(r) \geq 0, \forall r, \quad (22a)$$

$$A_0(r) + A_1(r) \geq 0, \forall r. \quad (22b)$$

Considering the most generic vector, the relation (4), and the metric (20), the non-vanishing components of Ricci tensor correction are given by

$$\bar{R}_{00} = -\frac{1}{2}e^{\alpha(r)-\beta(r)} \left[A'_1(r) - A_1^2(r) + \left(\frac{3}{2}\alpha'(r) - \frac{1}{2}\beta'(r) + \frac{2}{r} \right) A_1(r) \right], \quad (23a)$$

$$\bar{R}_{11} = \frac{1}{2} \left[3A'_1(r) + \left(\frac{1}{2}\alpha'(r) - \frac{3}{2}\beta'(r) + \frac{2}{r} \right) A_1(r) + e^{\beta(r)-\alpha(r)} A_0^2(r) \right], \quad (23b)$$

$$\bar{R}_{22} = \frac{1}{2}r^2 \left[e^{-\beta(r)} \left(A'_1(r) - A_1^2(r) + \left(\frac{1}{2}\alpha'(r) - \frac{1}{2}\beta'(r) + \frac{4}{r} \right) A_1(r) \right) + e^{-\alpha(r)} A_0^2(r) \right], \quad (23c)$$

$$\bar{R}_{33} = \sin^2(\theta) \bar{R}_{22}. \quad (23d)$$

Thus, the curvature scalar correction takes the form

$$\bar{R} = 3 \left[e^{-\beta(r)} \left(A'_1(r) - \frac{1}{2}A_1^2(r) + \left(\frac{1}{2}\alpha'(r) - \frac{1}{2}\beta'(r) + \frac{2}{r} \right) A_1(r) \right) + \frac{1}{2}e^{-\alpha(r)} A_0^2(r) \right]. \quad (24)$$

As far as the generalized Riemann curvature tensor is concerned, its components are computed in the Appendix A. These shall be relevant when computing the Kretschmann invariant in the next sections.

We now proceed to obtain the black hole-like solutions of this model in the form of generalized Schwarzschild and Reissner–Nordström types.

3 Schwarzschild-Like Black Hole

3.1 Vacuum

In this section, we analyze vacuum solutions, considering the two aforementioned possible realizations for the Weyl vector.

In this case, the field Equations (9) take the form of a pure $f(R)$ gravity with the Weyl connection:

$$(R_{\mu\nu} + \bar{\bar{R}}_{(\mu\nu)})F_1(\bar{R}) - \frac{1}{2}g_{\mu\nu}f_1(\bar{R}) = 0. \quad (25)$$

Taking the trace of these equations, we obtain

$$\bar{R}F_1(\bar{R}) - 2f_1(\bar{R}) = 0. \quad (26)$$

From this equation, two conclusions can be drawn. First of all, the model needs to be $f_1(\bar{R}) = \gamma\bar{R}^2$, with γ some integration constant. Secondly, we can also conclude that $\bar{R} = 0$. This also occurs for usual $f(R)$ gravity [35].

Please note that, when applying all these conclusions to constraint (8) and to relations (12), it is possible to see that all are trivially satisfied. Then, there are no longer any apparent restrictions on the Weyl vector, so we will analyze two different possible scenarios.

Considering the Ricci tensor corrections (23), the subsequent corrections for the scalar curvature (24), and the field Equation (9), we obtain the following:

$$R_{\mu\nu} + \bar{\bar{R}}_{\mu\nu} = 0, \quad (27a)$$

$$R + \bar{\bar{R}} = 0, \quad (27b)$$

with $\mu, \nu \in \{0, 1, 2\}$.

We now need to explore the possible ansatz for the Weyl vector field to solve the previous equations for the metric field free functions.

3.1.1 First Case: $A_\mu = (0, A(r), 0, 0)$

In this subsection, we will consider the simplest Weyl vector field $A_\mu = (0, A(r), 0, 0)$, with $A(r)$ an arbitrary function. Comparing the time-time and radial-radial components of the Equation (27a), we obtain the relation

$$(1 - rA(r))(\alpha'(r) + \beta'(r)) + r(A^2(r) + 2A'(r)) = 0. \quad (28)$$

We can further simplify this equation assuming that $\beta(r) = -\alpha(r) + \epsilon$, with ϵ some constant. Thus, we can find a solution for $A(r)$:

$$A(r) = \frac{2}{r + \omega}, \quad (29)$$

where $\omega > 0$, we call this the Weyl constant. We impose that ω is a positive constant to ensure that $A(r)$ is well defined and $A(r) > 0$, and no singularities or null length of the parallel transported vector appear, as can be seen in Equation (22a).

Thus, considering the field equations (27), it is easy to see that the solutions to the metric functions take the following form:

$$e^{\alpha(r)} = 1 - \frac{2M}{r} + \frac{2(\omega + 3M)}{\omega} \frac{r}{\omega} + \frac{\omega + 4M}{\omega} \left(\frac{r}{\omega}\right)^2, \quad (30a)$$

$$e^{\beta(r)} = \frac{1 + 6\left(\frac{M}{\omega}\right)}{1 - \frac{2M}{r} + \frac{2(\omega + 3M)}{\omega} \frac{r}{\omega} + \frac{\omega + 4M}{\omega} \left(\frac{r}{\omega}\right)^2}, \quad (30b)$$

where $M > 0$ is the black hole mass. We note that the relation between the components of the metric is $g_{11} = -\frac{1+6(\frac{M}{w})}{g_{00}}$. This numerical factor can be absorbed into a redefinition of the radial variable, namely, $r \rightarrow \tilde{r}$, such that $d\tilde{r}^2 = (1 + 6(\frac{M}{w})) dr^2$.

Moreover, if we are close to the black hole, we have $g_{00} \approx 1 - \frac{2M}{r}$, which is the same expression of the well-known Schwarzschild black hole in general relativity. On the other hand, if we are far enough, the metric component becomes $g_{00} \approx 1 + \frac{2(\omega+3M)}{\omega} \frac{r}{\omega} + \frac{\omega+4M}{\omega} (\frac{r}{\omega})^2$.

It is easy to see that, performing $g_{00} = 0$, we can obtain the event horizon, which occurs when $r_H = 2M \frac{\omega}{4M+\omega}$. We can, alternatively, write $r_H = 2\tilde{M}$, with $\tilde{M} = M \frac{\omega}{\omega+4M}$.

Analyzing, globally, $A(r)$, we can see that the Weyl vector has a good behavior, in the sense that $A(r)$ reaches a maximum value when $r = 0$, namely, $A(0) = \frac{2}{\omega}$, and asymptotically vanishes, i.e., for $r \rightarrow \infty$, we have $A(r) \rightarrow 0$.

In this gravity model under study, a Schwarzschild-like black hole can exist with a non-zero Ricci scalar. Although the total curvature scalar is zero, the Ricci scalar takes the form

$$R = -\frac{12(r + \omega) ((4M + \omega)r - M\omega)}{\omega^2(6M + \omega)r^2}. \quad (31)$$

We can obtain the global behavior for the Ricci scalar graphically in Figure 1. It is possible to see that, in the limit $r \rightarrow \infty$, the Ricci scalar $R \rightarrow -\frac{12(\omega+4M)}{\omega^2(\omega+6M)}$. We can also note that the minimum value of the Ricci scalar appears for $r_{\min} = 2M \frac{\omega}{3M+\omega}$ and this occurs outside the event horizon, $r_{\min} > r_H$. This minimum value is $R(r_{\min}) = -\frac{3(5M+\omega)^2}{M\omega^2(6M+\omega)}$, and the Ricci scalar in the event horizon is $R(r_H) = -\frac{3(4M+\omega)}{M\omega^2}$.

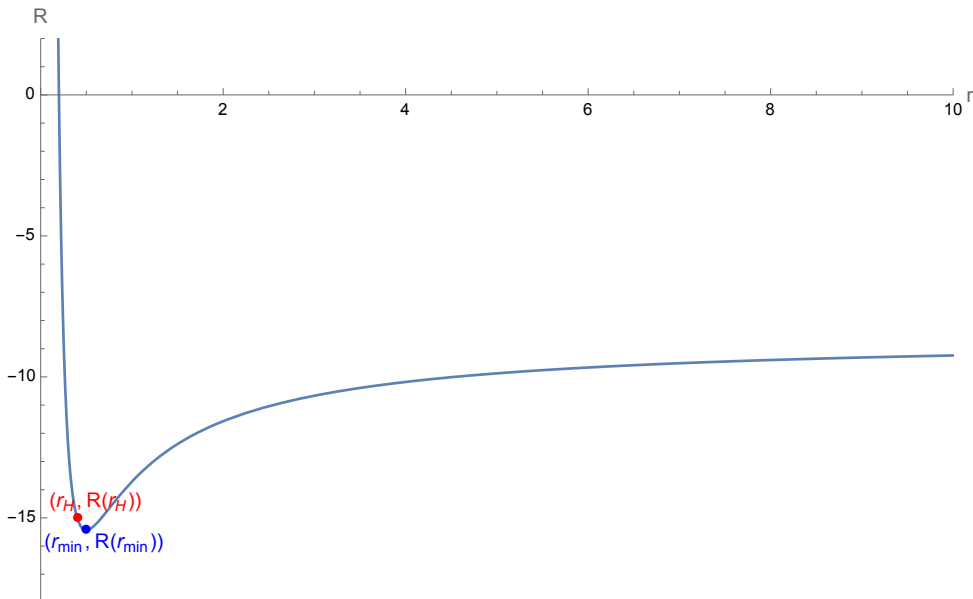


Figure 1: Global behavior of the standard Ricci scalar (built from the Levi-Civita part of the connection) as function of the distance, assuming $\omega = 1$ and $M = 1$.

In fact, we can assess whether the metric singularities are essential or removable by inspecting the Kretschmann invariant, which is the generalized Riemann squared $K = \bar{R}_{\mu\nu\sigma\rho} \bar{R}^{\mu\nu\sigma\rho}$, i.e., if those are real or due to the choice of the coordinate system. The Kretschmann was analyzed for the Kerr–Newman black hole in general relativity in Ref. [52], and for vector-tensor theories in Refs. [53, 54]. Moreover, some gravity models are devoid of $r = 0$ singularities when the atemporality mechanism is considered [55], the Hayward regularization of Schwarzschild black holes occurs [56], or quantum metric fluctuations are present in the form of a coupling of a scalar

field to the metric tensor [57], for instance. In our work, we do not pursue the latter avenues; thus, we shall compute the Kretschmann invariant to assess the nature of the singularities in our results. Thus, for this case, we obtain

$$K = \frac{48M^2}{r^6} \left(\frac{r + \omega}{6M + \omega} \right)^2. \quad (32)$$

It is possible to see that the Kretschmann invariant only diverges when $r = 0$ for any $M > 0$ and $\omega > 0$. Therefore, $r = 0$ is an essential singularity, i.e., a physical singularity that cannot be removed by a change of coordinates, in the center of the black hole. At the event horizon, the Kretschmann invariant takes the form $K_H = \frac{3(4M+\omega)^4}{4M^4\omega^4}$. Although the curvature in the event horizon may reach a considerable absolute magnitude, the invariant is always finite and positive.

Using the relation (15), we can deduce the geodesic equations. First of all, note that in this case, $f^\sigma = 0$, so the geodesic equations are the usual ones.

Let us consider $u^\sigma = (t(s), r(s), 0, 0)$. It is possible to obtain that the trajectory described by the geodesic can be given by

$$\frac{dr}{dt} = \frac{\Gamma_{00}^1 t^2 + \Gamma_{11}^1 r^2}{2\Gamma_{01}^0 tr}. \quad (33)$$

Considering the solution obtained in Equations (29) and (30), we can numerically solve the previous differential equation. For that, we will analyze three different regimes: $\omega = M$, $\omega \gg M$, and $\omega \ll M$. If $\omega \gg M$, it is possible to obtain, approximately, $g_{11} \approx -\frac{1}{g_{00}}$, $g_{00} \approx -\left(1 - \frac{2M}{r} + 2\frac{r}{\omega} + \left(\frac{r}{\omega}\right)^2\right)$. On the other hand, if $\omega \ll M$, it is possible to obtain the relations $g_{00} = -\left(1 - \frac{2M}{r} + 6\frac{M}{\omega}\frac{r}{\omega} + 4\frac{M}{\omega}\left(\frac{r}{\omega}\right)^2\right)$. Therefore, we expect that the non-metricity plays a very important role.

These three scenarios can be explored graphically. The numerical solutions of the geodesic equation, Equation (33), are shown in the next figures: Figure 2 for $\omega = M$, Figure 3 for $\omega \gg M$, and Figure 4 for $\omega \ll M$.

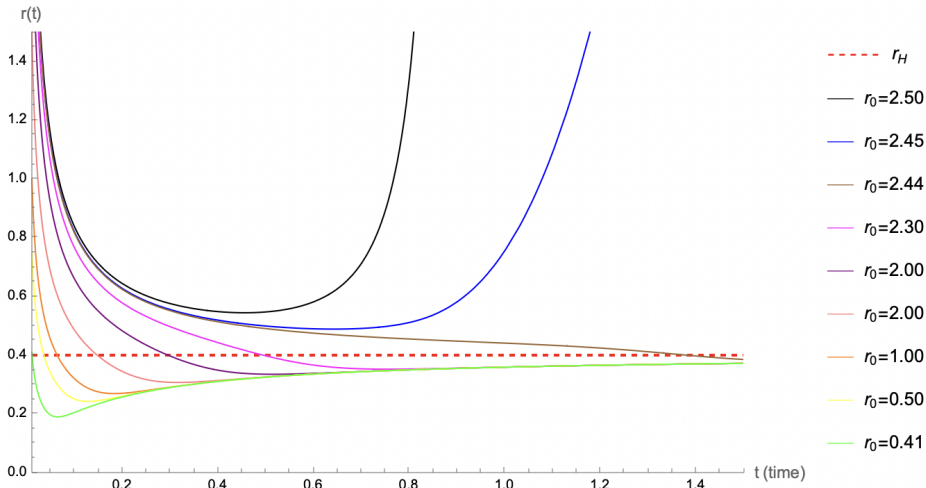


Figure 2: Geodesic representation of the Schwarzschild-like black hole (30), considering $\omega = M$, for the parameters $\omega = 1$ and $M = 1$. For the representation, the initial radius is denoted by r_0 , with initial time $t_0 = 0.01$.

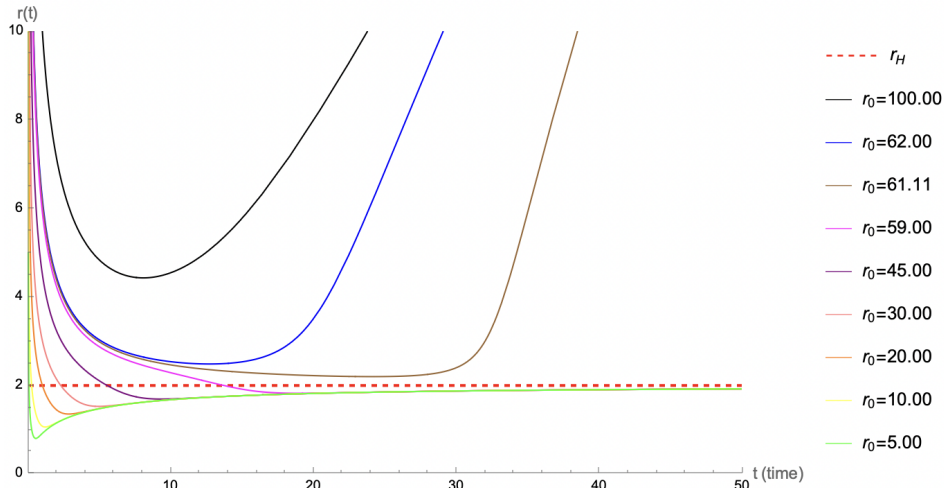


Figure 3: Geodesic representation of the Schwarzschild-like black hole (30), considering $\omega \gg M$, for the parameters $\omega = 10^4$ and $M = 1$. For the representation, the initial radius is denoted by r_0 , with initial time $t_0 = 0.01$.

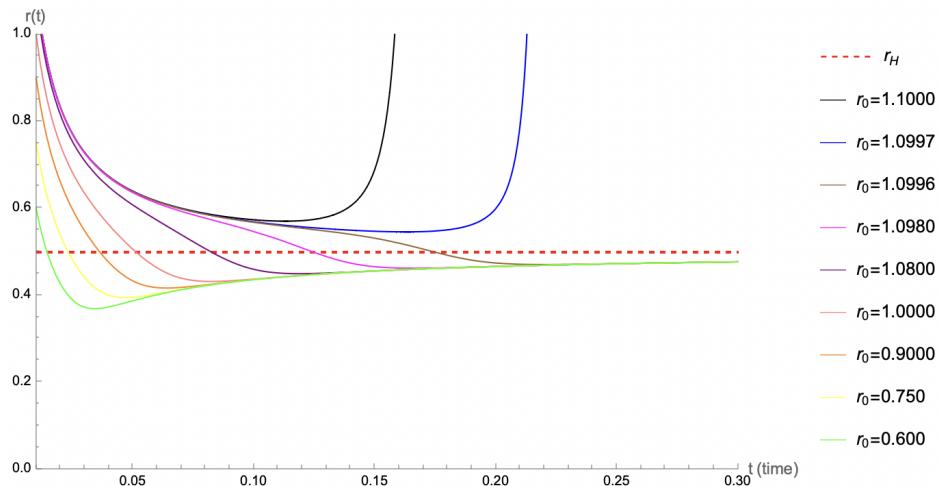


Figure 4: Geodesic representation of the Schwarzschild-like black hole (30), considering $\omega \ll M$, for the parameters $\omega = 1$ and $M = 10^2$. For the representation, the initial radius is denoted by r_0 , with initial time $t_0 = 0.01$.

Table 1 represents the estimated values for the event horizon, r_H , and the initial distance to the black hole (considering the initial time $t_0 = 0.01$), $r_{0,\text{crit}}$, after which, for initial distance $r_0 > r_{0,\text{crit}}$, the geodesic is no longer attracted to the black hole and diverges to infinity. For that, we consider three values for the mass, 10^{-2} , 1, and 10^2 , and six different values to the Weyl constant for each M . We now analyze the impact of each of the parameters.

M	ω	r_H	$r_{0,\text{crit}}$
10^{-2}	10^{-3}	4.87805×10^{-4}	4.898605×10^{-4}
	10^{-2}	4.0×10^{-3}	4.44686×10^{-3}
	10^{-1}	1.42857×10^{-2}	2.96460×10^{-2}
	1	1.92308×10^{-2}	5.55967×10^{-2}
	10^1	1.99203×10^{-2}	6.07338×10^{-2}
	10^2	1.99920×10^{-2}	6.12471×10^{-2}
1	10^{-2}	4.98753×10^{-3}	2.05553×10^{-3}
	10^{-1}	4.87805×10^{-2}	6.97344×10^{-2}
	1	0.4	2.440224
	10^1	1.42857	2.87911×10^1
	10^2	1.92308	5.57693×10^1
	10^3	1.99203	6.05870×10^1
10^2	10^{-1}	4.99875×10^{-2}	5.21649×10^{-2}
	1	4.98753×10^{-1}	1.09968
	10^1	4.87805	5.714214×10^1
	10^2	4.0×10^1	2.43480×10^3
	10^3	1.42857×10^2	2.87908×10^4
	10^4	1.92308×10^2	5.57693×10^4

Table 1: Estimated values for the event horizon, r_H , and the initial distance to the black hole, after which the geodesic is no longer attracted to the black hole and diverges to infinity, $r_{0,\text{crit}}$, considering different values for the mass and the Weyl parameters, M and ω , respectively.

In Figures 5–7, we represent an analysis of the relation between the mass of the black hole, the Weyl constant, the results of the event horizon, and the critical radius, $r_{0,\text{crit}}$. After that, for initial distance $r_0 > r_{0,\text{crit}}$ the geodesic is no longer attracted to the black hole and diverges to infinity. For that, 35 different values for the Weyl constant were considered, for each of the masses, and r_H and $r_{0,\text{crit}}$ were calculated numerically for each of the cases. Considering this analysis, we can conclude that the global behavior of both quantities is similar regardless of the mass of the black holes (small or large) of the used values for the Weyl constant. We can also conclude that there is an asymptotic behavior in the loglog representation for the event horizon and for the critical initial value of the distance for which the geodesic is no longer attracted to the black hole, and the higher the event horizon is, the higher this distance is found.

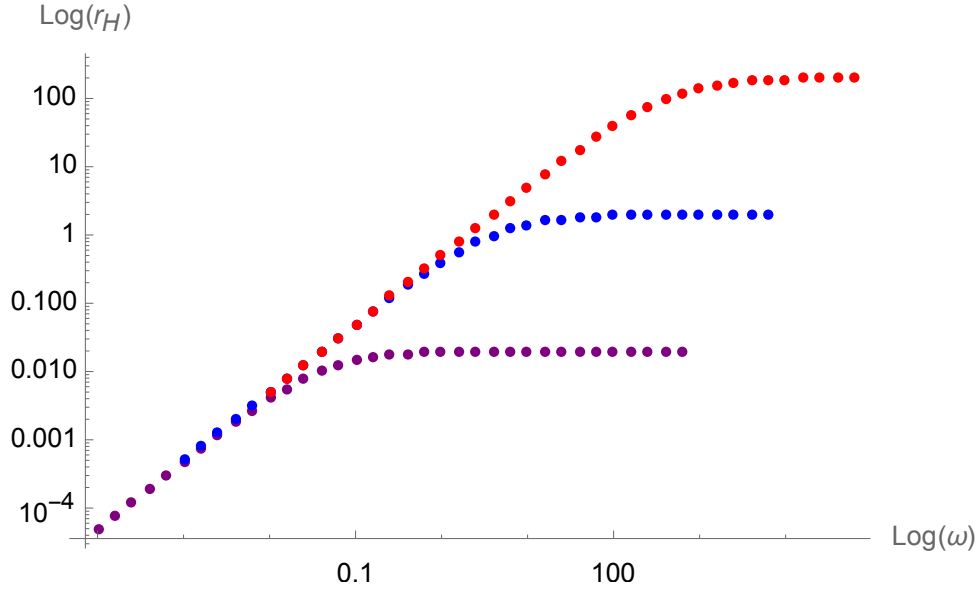


Figure 5: Behavior of r_H compared to ω , considering three different black hole masses: $M = 10^{-2}$, $M = 1$, and $M = 10^2$, represented by the colors purple, red, and blue, respectively. To capture all global behavior, 35 different values were considered for the ω parameter. For $M = 10^{-2}$, values were between 10^{-4} and 10^3 . For $M = 1$, values were between 10^{-3} and 10^4 . For $M = 10^2$, values were between 10^{-2} and 10^5 .

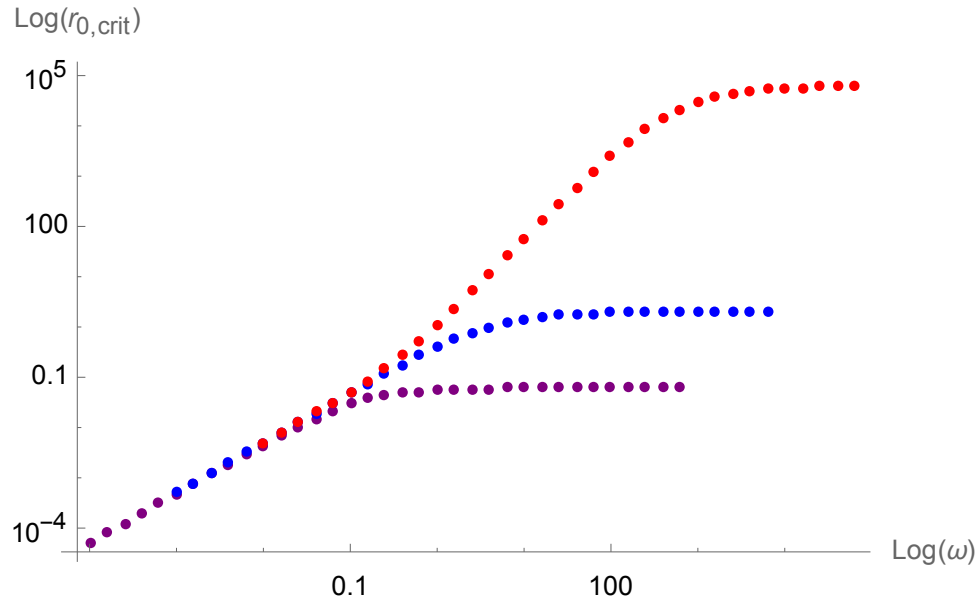


Figure 6: Behavior of $r_{0,\text{crit}}$ compared to ω , considering three different black hole masses: $M = 10^{-2}$, $M = 1$, and $M = 10^2$, represented by the colors purple, red, and blue, respectively. To capture all global behavior, 35 different values were considered for the ω parameter. For $M = 10^{-2}$, values were between 10^{-4} and 10^3 . For $M = 1$, values were between 10^{-3} and 10^4 . For $M = 10^2$, values were between 10^{-2} and 10^5 .

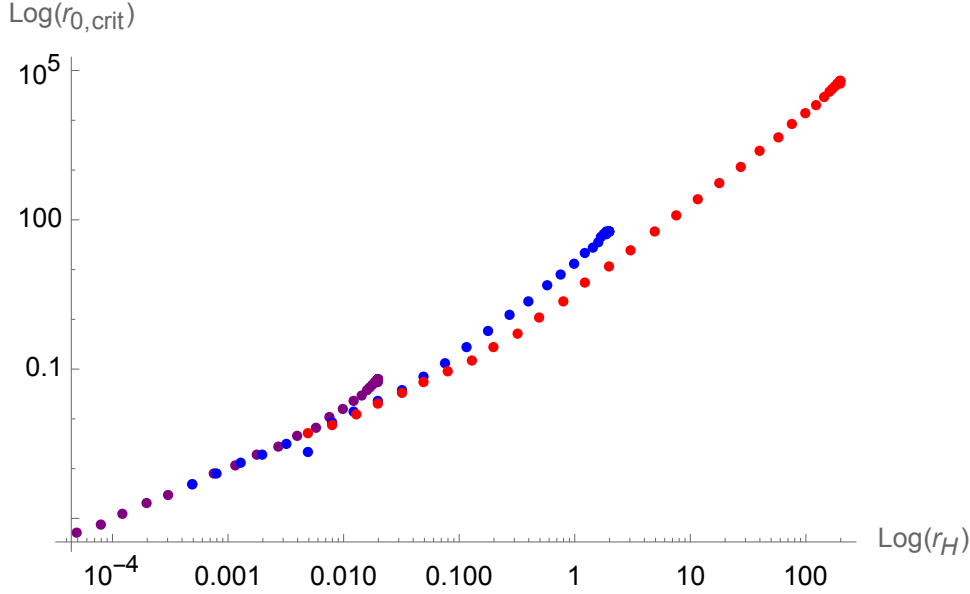


Figure 7: Behavior of $r_{0,\text{crit}}$ compared to r_H , considering three different black hole masses: $M = 10^{-2}$, $M = 1$, and $M = 10^2$, represented by the colors purple, red, and blue, respectively. To capture all global behavior, 35 different values were considered for the ω parameter. For $M = 10^{-2}$, values were between 10^{-4} and 10^3 . For $M = 1$, values were between 10^{-3} and 10^4 . For $M = 10^2$, values were between 10^{-2} and 10^5 .

3.1.2 Second Case: $A_\mu = (A_0(r), A_1(r), 0, 0)$

We now consider the second possible ansatz for the Weyl vector field, namely, $A_\mu = (A_0(r), A_1(r), 0, 0)$, with $A_0(r) \neq 0$ and $A_1(r) \neq 0$ being arbitrary functions that obey the constraint equation:

$$A_0'(r) + (A_1(r) - \alpha'(r))A_0(r) = 0. \quad (34)$$

Using this relation to $A_1(r)$ and comparing the time–time and the radial–radial components of Equation (27a), we obtain the following equation:

$$2rA_0''(r) - A_0'(r) (r (\alpha'(r) + \beta'(r)) - 4) = 0. \quad (35)$$

Analogously to the previous case, we assume that $\beta(r) = -\alpha(r) + \epsilon$, with ϵ some constant, together with the field equations (27), such that we find the following:

$$A_0(r) = \frac{1}{\omega} \left(1 - \frac{2M}{r} \right), \quad (36a)$$

$$A_1(r) = \frac{2r}{r^2 - 4\omega^2} \quad (36b)$$

$$e^{\alpha(r)} = 1 - \frac{2M}{r} + \frac{M}{2\omega} \left(\frac{r}{\omega} \right) - \frac{1}{4} \left(\frac{r}{\omega} \right)^2, \quad (36c)$$

$$e^{\beta(r)} = \frac{1}{1 - \frac{2M}{r} + \frac{M}{2\omega} \left(\frac{r}{\omega} \right) - \frac{1}{4} \left(\frac{r}{\omega} \right)^2}, \quad (36d)$$

where $M > 0$ is the black hole mass and ω is the Weyl constant. We note that the relation between the time–time and radial–radial components of the metric is $g_{11} = -\frac{1}{g_{00}}$, considering, without loss generality, $\epsilon = 0$.

It is easy to see that, by performing $g_{00} = 0$, we can obtain two event horizons, which occurs when $r_H^{(M)} = 2M$ and $r_H^{(\omega)} = 2|\omega|$. This result resembles the black hole and cosmological horizons discussion [58].

In order to understand the possible ω values, we will apply the constraint (22b) considering three different cases: $\omega = M$, $|\omega| > M$, and $|\omega| < M$. In the first case, considering $\omega = M$, we only have one event horizon, $R_H = 2M$. The constraint (22b) is automatically satisfied outside the event horizon for any $M > 0$. In the second case, $|\omega| > M$, we have two event horizons and the external one is the $r_H^{(\omega)}$. The constraint (22b) is satisfied for any $r > r_H^{(\omega)}$ if and only if $\omega > 0$. Finally, when $|\omega| < M$, we also have two event horizons, and the external one is $r_H^{(M)}$. The constraint (22b) is satisfied for any $r > r_H^{(M)}$ also if and only if $\omega > 0$. Therefore, in general, we have to impose that $\omega > 0$.

Analyzing, globally, the Weyl vector, we can see that $A_0(r) \rightarrow \frac{1}{\omega}$ and $A_1(r) \rightarrow 0$, when $r \rightarrow \infty$. In fact, if we require space-time to be asymptotically flat, then $\omega \gg 1$; but if we expect that at infinity we can have non-zero background, then we see that the vector field contributes cosmologically at infinity with $A_0 = 1/\omega$.

In this gravity model under study, a Schwarzschild-like black hole can exist with a non-zero Ricci scalar. Although the total curvature scalar is zero, the Ricci scalar takes the form

$$R = \frac{3(r - M)}{\omega^2 r}. \quad (37)$$

We can obtain the global behavior for the Ricci scalar graphically in Figure 8. It is possible to see that, in the limit $r \rightarrow \infty$, the Ricci scalar $R \rightarrow \frac{3}{\omega^2}$. We also can note that the Ricci curvature is zero when $r = M$, i.e., on the surface of the black hole. When $\omega > M$, the Ricci scalar in the external event horizon is given by $R(r_H^{(\omega)}) = \frac{3(2\omega - M)}{2\omega^3}$. When $\omega \leq M$, the Ricci scalar in the external event horizon is given by $R(r_H^{(M)}) = \frac{3}{2\omega^2}$.

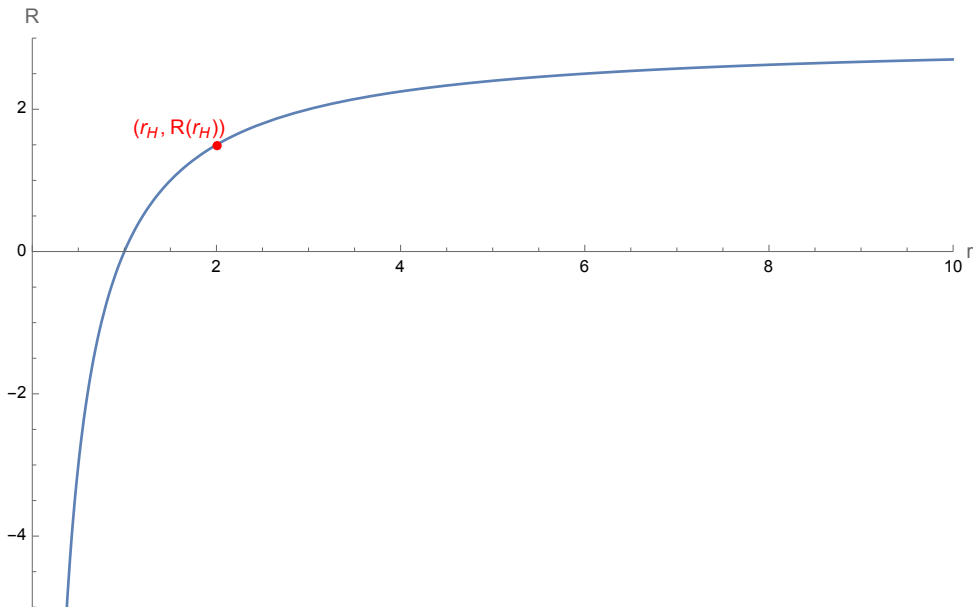


Figure 8: Global behavior of the standard Ricci scalar (built from the Levi-Civita part of the connection) as function of the distance, assuming $\omega = 1$ and $M = 1$.

In order to assess the nature of the singularities in this result, we compute the Kretschmann invariant. Thus, for this case, we obtain

$$K = \frac{48M}{r^6} \left(\frac{4M\omega^2(47 - 2Mr + r^2) - r^2(44M - 2r(1 + M^2) + Mr^2)}{192\omega^2} \right) \quad (38)$$

It is possible to see that the Kretschmann invariant only diverges when $r = 0$ for any $M > 0$ and $\omega > 0$. Therefore, $r = 0$ is an essential singularity in the center of the black

hole. At the event horizons, the Kretschmann invariant takes the forms $K_H^{(\omega)} = \frac{M(3M+4\omega)}{64\omega^6}$ and $K_H^{(M)} = \frac{47\omega^2-40M^2}{64\omega^2M^2}$. Although the curvature in the event horizon may reach a considerable absolute magnitude, the invariant is always finite. When $\omega > M$, the invariant takes positive values at both the external, $r_H^{(\omega)}$, and the internal, $r_H^{(M)}$, event horizon. When $\omega = M$, there only exists one event horizon and the invariant is also positive. When $\omega < M$, in the internal event horizon, $r_H^{(\omega)}$, the invariant is positive. In the external event horizon, $r_H^{(M)}$, the invariant is positive when $\sqrt{\frac{40}{47}}M < \omega < M$, is zero when $\omega = \sqrt{\frac{40}{47}}M$, and is negative when $\omega < \sqrt{\frac{40}{47}}M$.

Using the relation of Equation (15), we derive the geodesics equation. Firstly, we note that in this case, $f^\sigma = 0$, so the geodesics equation is the usual one from general relativity.

Let us further consider $u^\sigma = (t(s), r(s), 0, 0)$. Therefore, the trajectory described by the geodesics can be given by

$$\frac{dr}{dt} = \frac{\Gamma_{00}^1 t^2 + \Gamma_{11}^1 r^2}{2\Gamma_{01}^0 tr}. \quad (39)$$

The numerical solutions of the geodesic equation, Equation (39), are shown in the next figures, considering three different scenarios: Figure 9 for $\omega = M$, Figure 10 for $\omega \gg M$, and Figure 11 for $\omega \ll M$.

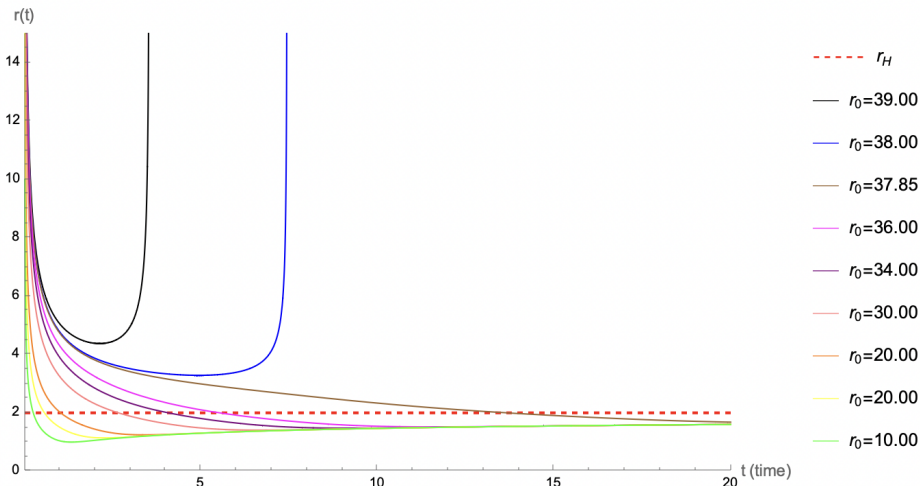


Figure 9: Geodesic representation of the Schwarzschild-like black hole (36), considering $\omega = M$, for the parameters $\omega = 1$ and $M = 1$. For the representation, the initial radius is denoted by r_0 , with initial time $t_0 = 0.01$.

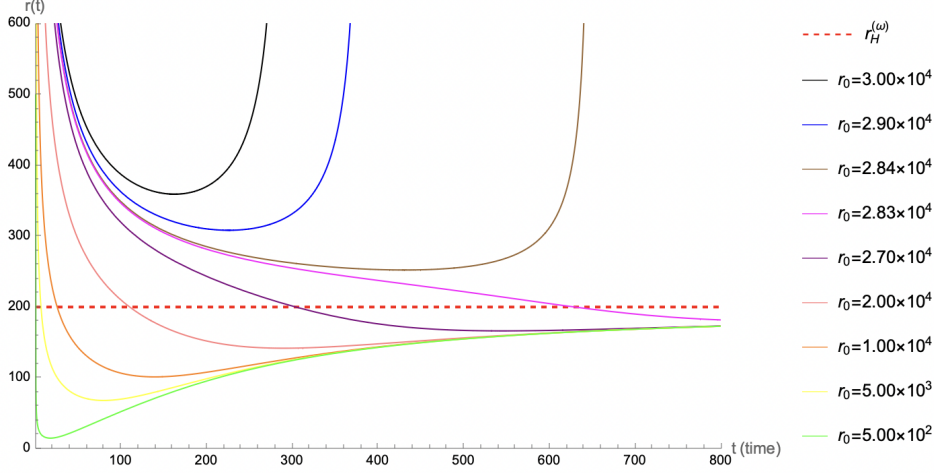


Figure 10: Geodesic representation of the Schwarzschild-like black hole (36), considering $\omega \gg M$, for the parameters $\omega = 10^2$ and $M = 1$. For the representation, the initial radius is denoted by r_0 , with initial time $t_0 = 0.01$

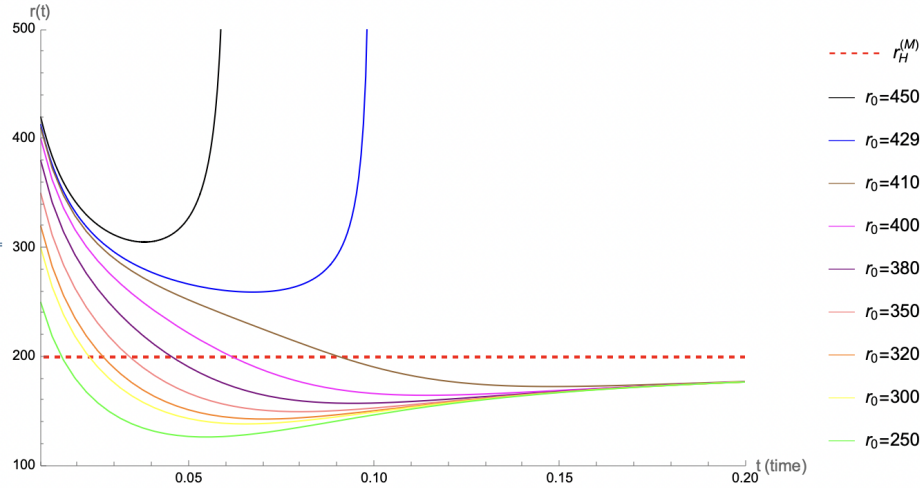


Figure 11: Geodesic representation of the Schwarzschild-like black hole (36), considering $\omega \ll M$, for the parameters $\omega = 1$ and $M = 10^2$. For the representation, the initial radius is denoted by r_0 , with initial time $t_0 = 0.01$.

We complement the analysis with a table, namely, Table 2, which represents the estimated values for the external event horizon, $r_{H,\text{ext}}$ ($r_H^{(\omega)}$ or $r_H^{(M)}$), depending on the value of the parameters), and the initial distance to the black hole (considering the initial time $t_0 = 0.01$), $r_{0,\text{crit}}$; after that, for initial distance $r_0 > r_{0,\text{crit}}$, the geodesic is no longer attracted to the black hole and diverges to infinity. For that, we consider three types of masses, 10^{-2} , 1, and 10^2 , and six different values to the Weyl constant for each M . Here, we intend to analyze the impact of each of the parameters.

M	ω	$r_{H,\text{ext}}$	$r_{0,\text{crit}}$
10^{-2}	10^{-3}	2.0×10^{-2}	2.03962×10^{-2}
	10^{-2}	2.0×10^{-2}	4.74587×10^{-2}
	10^{-1}	2.0×10^{-1}	9.40337×10^{-1}
	1	2.0	2.84252×10^1
	10^1	2.0×10^1	8.94872×10^2
	10^2	2.0×10^2	2.82857×10^4
1	10^{-2}	2.0	2.03925
	10^{-1}	2.0	4.12739
	1	2.0	3.79018×10^1
	10^1	2.0×10^1	9.17359×10^2
	10^2	2.0×10^2	2.83548×10^4
	10^3	2.0×10^3	8.94650×10^5
10^2	10^{-1}	2.0×10^2	2.03924×10^2
	1	2.0×10^2	4.12172×10^2
	10^1	2.0×10^2	3.41783×10^3
	10^2	2.0×10^2	3.77465×10^4
	10^3	2.0×10^3	9.17119×10^5
	10^4	2.0×10^4	2.83541×10^7

Table 2: Estimated values for the external event horizon, $r_{H,\text{ext}}$, and the initial distance to the black hole, after which the geodesic is no longer attracted to the black hole and diverges to infinity, $r_{0,\text{crit}}$, considering different values for the mass and the Weyl parameters, M and ω , respectively.

In Figures 12–14, we represent an analysis of the relation between the mass of the black hole, the Weyl constant, the results of the event horizon, and the critical radius, $r_{0,\text{crit}}$; after that, for initial distance $r_0 > r_{0,\text{crit}}$, the geodesic is no longer attracted to the black hole and diverges to infinity. For that, we considered 35 different values for the Weyl constant, for each of the masses, and $r_{H,\text{ext}}$ and $r_{0,\text{crit}}$ were calculated numerically for each of the cases. Due to the limitations of numerical simulations, we cannot plot much further (higher values for ω); therefore, we cannot directly compare to the general behavior from the first ansatz for the Weyl vector field. We note, however, that this case has two horizons (possibly a black hole and a cosmological ones; see, e.g., Refs. [58, 46]).

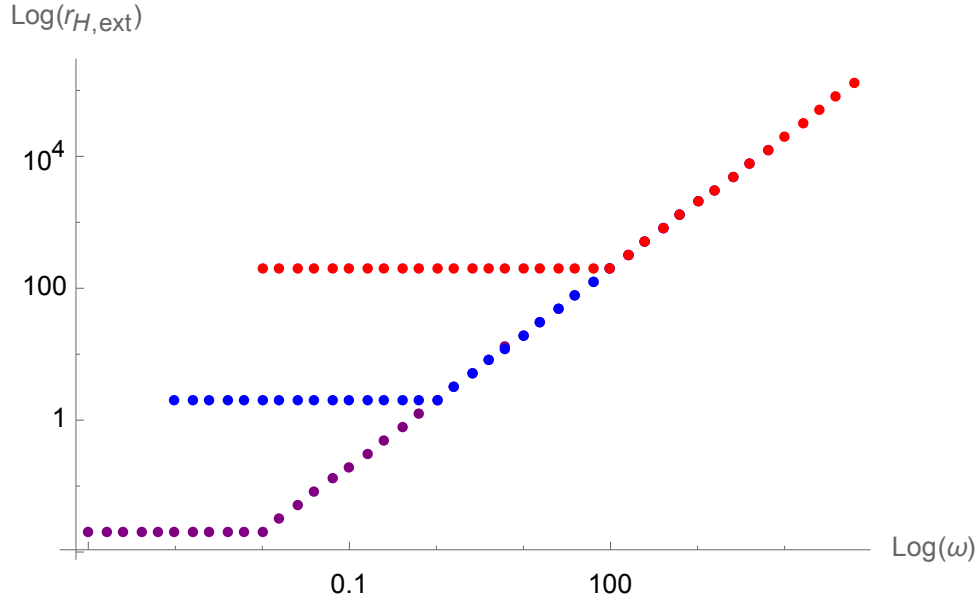


Figure 12: Behavior of $r_{H,\text{ext}}$ compared to ω , considering three different black hole masses: $M = 10^{-2}$, $M = 1$, and $M = 10^2$, represented by the colors purple, red, and blue, respectively. To capture all global behavior, 35 different values were considered for the ω parameter. For $M = 10^{-2}$, values were between 10^{-4} and 10^3 . For $M = 1$, values were between 10^{-3} and 10^4 . For $M = 10^2$, values were between 10^{-2} and 10^5 .

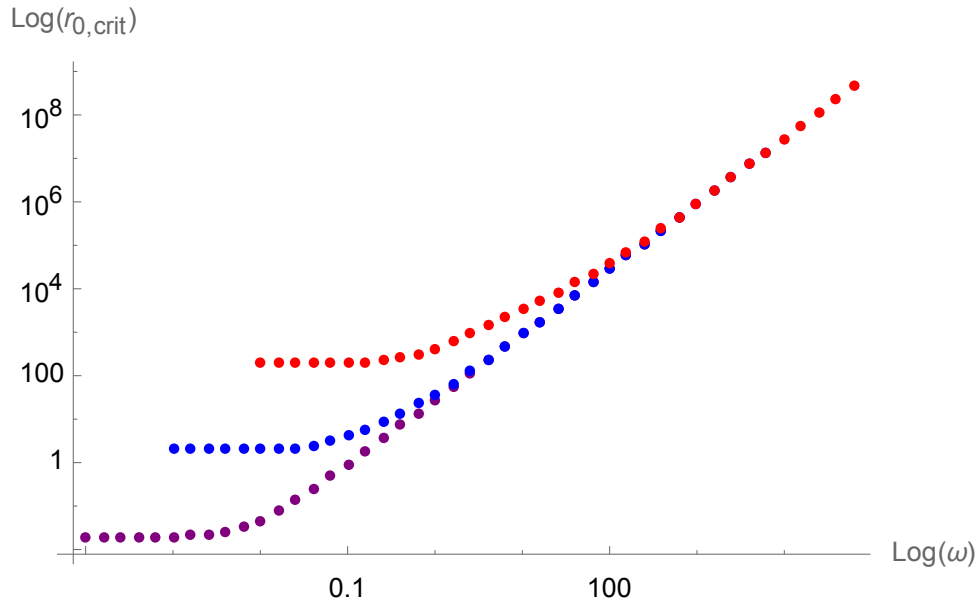


Figure 13: Behavior of $r_{0,\text{crit}}$ compared to ω , considering three different black hole masses: $M = 10^{-2}$, $M = 1$, and $M = 10^2$, represented by the colors purple, red, and blue, respectively. To capture all global behavior, 35 different values were considered for the ω parameter. For $M = 10^{-2}$, values were between 10^{-4} and 10^3 . For $M = 1$, values were between 10^{-3} and 10^4 . For $M = 10^2$, values were between 10^{-2} and 10^5 .

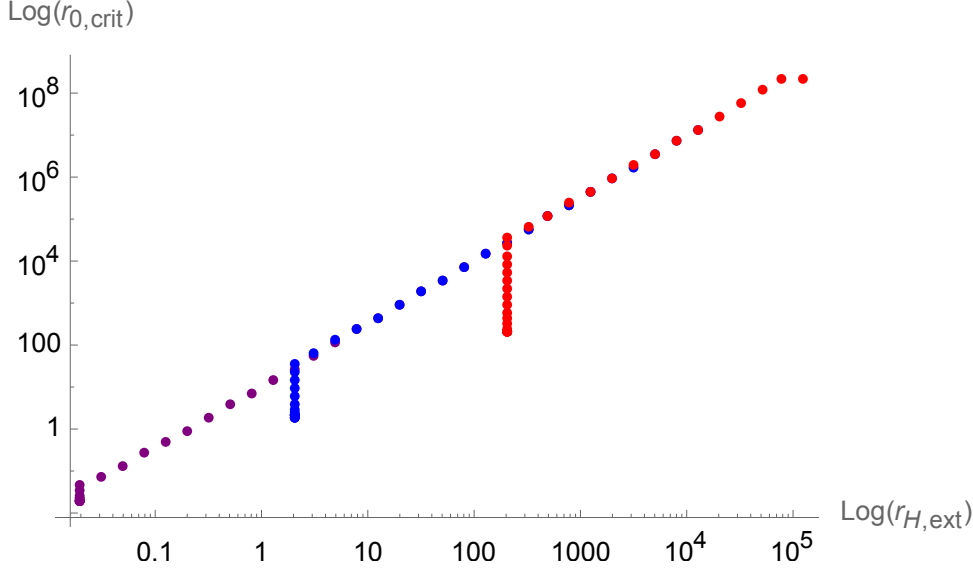


Figure 14: Behavior of $r_{H,\text{ext}}$ compared to $r_{0,\text{crit}}$, considering three different black hole masses: $M = 10^{-2}$, $M = 1$, and $M = 10^2$, represented by the colors purple, red, and blue, respectively. To capture all global behavior, 35 different values were considered for the ω parameter. For $M = 10^{-2}$, values were between 10^{-4} and 10^3 . For $M = 1$, values were between 10^{-3} and 10^4 . For $M = 10^2$, values were between 10^{-2} and 10^5 .

3.2 Cosmological Constant Background

In this section, we will analyze the black hole solutions when the matter Lagrangian density is non-vanishing. For simplicity and in order to grasp the first non-trivial solution, we shall consider it in the form of a cosmological constant, i.e., a constant energy density. Considering $\mathcal{L}^{(\Lambda)} = -2\Lambda$, the energy-momentum tensor components are given by

$$T_{\mu\nu}^{(\Lambda)} = -2\Lambda g_{\mu\nu}. \quad (40)$$

The field Equation (9) takes the form

$$\bar{R}_{\mu\nu} (F_1(\bar{R}) - 2\Lambda F_2(\bar{R})) - \frac{1}{2} (f_1(\bar{R}) - 2\Lambda f_2(\bar{R})) = 0. \quad (41)$$

Taking the trace of these equations, we obtain the relation

$$f_1(\bar{R}) - 2\Lambda f_2(\bar{R}) = \gamma \bar{R}^2 + \xi, \quad (42)$$

where γ and ξ are constants.

Thus, the field equations are

$$\bar{R}_{\mu\nu} - \frac{1}{4} g_{\mu\nu} \bar{R} = 0, \quad (43)$$

that implies that

$$\bar{R}_{\mu\nu} = 0, \quad (44)$$

$$\bar{R} = 0. \quad (45)$$

It is straightforward to verify that, taking Equations (42) and (45) into account, both constraint Equation (8) and the non-conservation law (12) are automatically satisfied for any vector field A_λ . Therefore, the vacuum solutions found above are also solutions when we consider a

cosmological constant background. Therefore, we can interpret this result as stemming from the mathematical reparametrization, namely, $f(\bar{R}) = f_1(\bar{R}) - 2\Lambda f_2(\bar{R})$ in Equation (42). However, as discussed in Ref. [40], physically, these two models are distinct, as one has a physical meaning for the cosmological constant-like Lagrangian (the energy from vacuum). Thus, we can relate this ‘‘cosmological constant’’ with a cosmological constant appearing as an integration constant of the field equations. The non-minimal coupling model has an advantage of allowing for contributing to an explanation of the so-called cosmological constant problem.

3.3 Thermodynamics

We now evaluate some thermodynamics quantities for the black hole solutions found in this paper for the non-minimally coupled Weyl connection gravity model. We closely follows Refs. [48, 49, 46] in order to compute such quantities.

Therefore, for the metric (20), the black hole temperature from the quantum tunneling method (which is equivalent to the Hawking method [48], and we denote by the superscript ‘‘BH’’) is given by

$$T^{(BH)} = \frac{\sqrt{(e^{\alpha(r_{H,\text{ext}})})' (e^{-\beta(r_{H,\text{ext}})})'}}{4\pi} = \frac{\sqrt{-\alpha'(r_{H,\text{ext}})\beta'(r_{H,\text{ext}})e^{\alpha(r_{H,\text{ext}})-\beta(r_{H,\text{ext}})}}}{4\pi}. \quad (46)$$

The black hole entropy is given by

$$S^{(BH)} = \int \frac{dM}{T^{(BH)}(M)} \quad (47)$$

and the black hole heat capacity at constant volume takes the form

$$C_V^{(BH)} = T^{(BH)} \frac{\partial S^{(BH)}}{\partial T^{(BH)}} = T^{(BH)} \frac{\partial S^{(BH)}}{\partial r_{H,\text{ext}}} \left(\frac{\partial T^{(BH)}}{\partial r_{H,\text{ext}}} \right)^{-1}. \quad (48)$$

We can also derive such quantities from the so-called ‘‘area approach’’. Thus, the area temperature reads as follows:

$$T^{(A)} = \frac{r_{H,\text{ext}} - r_{H,\text{int}}}{4\pi r_{H,\text{ext}}^2}. \quad (49)$$

Analogously, the area entropy is

$$S^{(A)} = \frac{A(r_{H,\text{ext}})}{4}, \quad (50)$$

and the area specific heat capacity is

$$C_V^{(A)} = T^{(A)} \frac{\partial S^{(A)}}{\partial T^{(A)}} = T^{(A)} \frac{\partial S^{(A)}}{\partial r_{H,\text{ext}}} \left(\frac{\partial T^{(A)}}{\partial r_{H,\text{ext}}} \right)^{-1}. \quad (51)$$

When both definitions do not coincide, then we need to modify the first law of thermodynamics [59, 60, 48]; likewise, the non-minimal coupling model has bearings on the second law [16], such that

$$dM = TdS \implies T^{(A)} dS^{(A)} = T^{(BH)} dS^{(BH)}, \quad (52)$$

from which one can parametrize the following:

$$T^{(BH)} dS^{(BH)} = L^{(A)} dM, \quad (53)$$

where $L^{(A)} = T^{(A)} \frac{dS^{(A)}}{dM}$ is a function to be determined [48].

Finally, for both definitions, the free energy stems from

$$F = M - TS. \quad (54)$$

We now apply these definitions to each solution found for the Schwarzschild-like black holes.

3.3.1 Schwarzschild-Like Black Hole: First Case

Considering the solution (30), the previous thermodynamical quantities read as follows:

$$T^{(BH)} = T_0 \left(1 + 6\frac{M}{\omega}\right)^{-3/2}, \quad (55a)$$

$$S^{(BH)} = \frac{8\pi}{9} \left(1 + 6\frac{M}{\omega}\right)^{-3/2} (3M + \omega)(6M + \omega), \quad (55b)$$

$$C_V^{(BH)} = C_0 \left(1 + 6\frac{M}{\omega}\right)^{-3/2} \frac{6M + \omega}{\omega - 3M}, \quad (55c)$$

where $T_0 = \frac{1}{8\pi M}$ and $C_0 = -8\pi M^2$ are the Hawking temperature and the heat capacity at constant volume for the usual Schwarzschild black hole, respectively. This expression for the specific heat means that the black hole is stable for $\omega > 3M$, and unstable for $\omega < 3M$, as the black hole will evaporate, leaving a stable cold remnant, in contrast with standard Schwarzschild black holes in general relativity, which are always unstable as their temperatures increase as they absorb mass. The specific heat diverges at $\omega = 3M$ despite not corresponding to the maximum temperature, which is a decreasing function of the mass and has a maximum at zero mass, i.e., $T_{\max} = T_0$. Nonetheless, this might signal the existence of a thermodynamical critical transition point.

Using the relation (54), the free energy considering the tunneling method takes the form

$$F^{(BH)} = - \left(M + \omega + \frac{\omega^2}{9M} \right), \quad (56)$$

which can be minimized when $\omega = 0$ and $M \neq 0$. Thus, the system in the quantum tunneling description can be globally stable, as it allows for non-vanishing masses to minimize its free energy.

We now proceed to compute the previous quantities using the area method. We draw our attention to the fact that there is only one event horizon, namely, $r_H = 2M\frac{\omega}{4M+\omega}$, thus being formally equivalent to impose $r_{H,int} = 0$.

Therefore, the area temperature, the area entropy, and the area specific heat capacity at constant volume are given by

$$T^{(A)} = T_0 \frac{4M + \omega}{\omega}, \quad (57a)$$

$$S^{(A)} = 4\pi \left(\frac{M\omega}{4M + \omega} \right)^2, \quad (57b)$$

$$C_V^{(A)} = C_0 \left(\frac{\omega}{4M + \omega} \right)^2. \quad (57c)$$

As we can see, the area specific heat capacity at constant volume is always positive definite; thus, the system is locally stable for all values of the mass and of the Weyl constant. Furthermore, using the relation (54), the free energy considering the ‘‘area approach’’ takes the form

$$F^{(A)} = \frac{M(8M + \omega)}{2(4M + \omega)}, \quad (58)$$

which is minimized for $M = 0$; thus, the system is globally unstable in the area method.

As the area and quantum tunneling methods lead to different results, the first law must be revisited [48]. In this case, the function $L^{(A)} = \frac{\omega^2}{(4M+\omega)^2}$.

3.3.2 Schwarzschild-Like Black Hole: Second Case

Taking into account the solution (36) and applying the expression (46), considering the external event horizon, it is possible to see that $T^{(BH)}$ is purely imaginary and diverges, which is non-physical:

$$T^{(BH)} = \frac{i}{2\pi r} \left| \frac{r^3 - M(r^2 + 4\omega^2)}{(r - 2M)(r^2 - 4\omega^2)} \right|. \quad (59)$$

If we instead compute the thermodynamical quantities via the ‘‘area approach’’, we have three cases to analyze.

The first case corresponds to $\omega < M$, for which the two event horizons read $r_{H,\text{int}} = 2\omega$ and $r_{H,\text{ext}} = 2M$. Thus, the area temperature, the area entropy, and the specific heat at constant volume are

$$T^{(A)} = T_0 \left(1 - \frac{\omega}{M}\right), \quad (60a)$$

$$S^{(A)} = 4\pi M^2, \quad (60b)$$

$$C_V^{(A)} = C_0 \frac{\omega - M}{2\omega - M}. \quad (60c)$$

As we can see, the area temperature is always positive and does not diverge, and the area specific heat is positive when $\omega < M < 2\omega$, negative when $2\omega < M$, and diverges at $M = 2\omega$. This critical point does not correspond to the maximum value of the temperature that occurs for a vanishing Weyl constant and has the value of $T_{\text{max}} = T_0$. Nevertheless, one can see that the system is locally unstable for negative values of the specific heat, and stable for positive ones. Therefore, the free energy is given by

$$F^{(A)} = \frac{\omega + M}{2}, \quad (61)$$

which is minimized for both vanishing mass and Weyl constant.

As for the second case, namely, when $\omega > M$, we have $r_{H,\text{int}} = 2M$ and $r_{H,\text{ext}} = 2\omega$. Thus, the area temperature, entropy, and specific heat are given by

$$T^{(A)} = T_0 \frac{M}{\omega} \left(1 - \frac{M}{\omega}\right), \quad (62a)$$

$$S^{(A)} = 4\pi\omega^2, \quad (62b)$$

$$C_V^{(A)} = C_0 \left(\frac{\omega}{M}\right)^2 \frac{M - \omega}{2M - \omega}. \quad (62c)$$

In this case, the temperature is always positive and does not diverge, and the specific heat is positive when $M < \omega < 2M$ and this Schwarzschild-like black hole evaporates to a locally stable cold remnant, negative when $2M < \omega$, and diverges for $\omega = 2M$. In this case, the critical point of the specific heat corresponds to the temperature maximum, $T_{\text{max}} = \frac{T_0}{4}$. Finally, the free energy is given by

$$F^{(A)} = \frac{3M - \omega}{2}, \quad (63)$$

which can be positive, null, or negative.

The third case corresponds to $\omega = M$, for which $r_H = 2M$. Therefore, analogously to the other cases, we can compute the following:

$$T^{(A)} = T_0, \quad (64a)$$

$$S^{(A)} = 4\pi M^2, \quad (64b)$$

$$C_V^{(A)} = C_0. \quad (64c)$$

Finally, the free energy is

$$F^{(A)} = \frac{M}{2}, \quad (65)$$

which is minimized only for $M = 0$; thus, the system is globally unstable.

This case reproduces the behavior of general relativity's non-rotating black holes. Since the area and quantum tunneling methods lead to different results in this second case as well, the first law must be revisited [48]. However, in this case, it is not possible to fully determine the function $L^{(A)}$ since the quantum tunneling leads to divergent quantities.

4 Reissner–Nordström-Like Black Hole

In this section, we will analyze black hole solutions of the form of Reissner–Nordström, i.e., black holes which are static and have mass and electric charge. In order to describe the gravitational field outside a charged, non-rotating, spherically symmetric body, we consider the electrostatic four-potential $\Phi_\mu = (-\phi(r), 0, 0, 0)$, with $\phi(r)$ as the scalar potential. Using the relation (18), it is possible to see that $\mathcal{L}^{(EM)} = \frac{1}{2}e^{-\alpha(r)-\nu(r)}\phi'(r)^2$, and the energy momentum-tensor is such that

$$T^{(EM)\mu}_\nu = \text{diag}(-1, -1, 1, 1)\frac{1}{2}e^{-\alpha(r)-\beta(r)}\phi'(r)^2. \quad (66)$$

Applying the previous result into the Maxwell Equation (19), it follows that

$$\phi'(r) = -e^{\frac{1}{2}(\alpha(r)+\beta(r))}\frac{c_1}{f_2(\bar{R})r^2}, \quad (67)$$

with c_1 being some constant, which we identify with the electric charge, Q , in analogy with the general relativity result.

Analogously to the Schwarzschild-like solutions, we shall look into vacuum and the first simplest contribution from non-vacuum Lagrangian density.

4.1 Vacuum Background

We now consider a vacuum background. Thus, the contribution to the energy-momentum tensor is given only by the black hole geometry seen from the infinity as a point charge.

First of all, it should be noted that $\Theta(\bar{R}) \neq 0$. Otherwise, Equation (11) implies zero energy-momentum tensor, since $T^{(EM)} = 0$. Therefore, the only applicable Weyl vector is the radial one, Equation (21a).

From the trace of the field Equation (10), we have

$$f_1(\bar{R}) = \frac{1}{2}\bar{R}\Theta(\bar{R}). \quad (68)$$

Applying this result, together with the fact that $F_1(\bar{R}) = \frac{df_1(\bar{R})}{d\bar{R}}$ and the constraint (8), we obtain

$$F_1(\bar{R}) = \frac{1}{2}\left(1 - A(r)\frac{\bar{R}}{\bar{R}'}\right)\Theta(\bar{R}), \quad (69)$$

when $\bar{R}' \neq 0$.

Using this relation, together with $\Theta(\bar{R}) = F_1(\bar{R}) + \mathcal{L}F_2(\bar{R})$ and the non-conservation equation to energy-momentum tensor (12), it is possible to observe that $f_2(\bar{R}) = 0$. Thus, we conclude that it is not possible to derive a charged black hole solution, in a vacuum, for any static and spherical metric in the model under study.

If $\bar{R}' = 0$, it is also impossible to obtain a black hole solution. In fact, $\bar{R}' = 0$ implies that the curvature scalar is constant, so $\Theta(\bar{R})$ is also constant. From the constraint (8), this implies that $A(r) = 0$.

4.2 Cosmological Constant Background

We now consider a charged black hole immersed in a cosmological constant background. Then, the Lagrangian density is given by $\mathcal{L} = \mathcal{L}^{(EM)} + \mathcal{L}^{(\Lambda)}$ and the components of the energy momentum tensor are $T_{\mu\nu} = T_{\mu\nu}^{(EM)} + T_{\mu\nu}^{(\Lambda)}$, as described above.

It should be noted that, again, $\Theta(\bar{R}) \neq 0$. Otherwise, Equation (11) implies zero energy-momentum tensor, since $T^{(EM)} = 0$. Therefore, the only viable ansatz for the Weyl vector is the radial one, Equation (21a).

By combining all trace-free Equation (11), it is possible to find a similar equation to (28). Therefore, we will use the same relation $\beta(r) = -\alpha(r) + \epsilon$. With this assumption, it is possible to see that the solution to $A(r)$ is, again,

$$A(r) = \frac{2}{r + \omega}, \quad (70)$$

with $\omega > 0$.

Thus, from (8), we obtain

$$\Theta(\bar{R}) = \frac{\xi}{(r + \omega)^2}, \quad (71)$$

with ξ some integration constant that we will define later.

Using this result in all previous equations, it is possible to obtain that the appropriated model is given by

$$f_1(\bar{R}) = \gamma \bar{R}^2 + 2\Lambda\zeta \quad (72a)$$

$$f_2(\bar{R}) = \zeta, \quad (72b)$$

where $\gamma = \xi \frac{(6\tilde{Q}^2 + 6M\omega + \omega^2)}{72\tilde{Q}^2}$, $\xi = \frac{\omega^2}{4}\zeta$, ζ is some constant, and \tilde{Q} is the dressed charge such that Equation (67) gives

$$\phi(r) = \frac{\tilde{Q}}{r}, \quad (73)$$

and we have the relation

$$Q^2 = \zeta^2 \tilde{Q}^2 \left(1 + 6 \left(\frac{M}{\omega} + \frac{\tilde{Q}^2}{\omega^2} \right) \right)^{-1}, \quad (74)$$

where Q is the usual charge.

The metric solution to this problem is given by

$$e^{\alpha(r)} = 1 - \frac{2M}{r} + \frac{\tilde{Q}^2}{r^2} + \frac{2(\omega^2 + 3M\omega + 2\tilde{Q}^2)}{\omega^2} \frac{r}{\omega} + \frac{4M + \omega}{\omega} \left(\frac{r}{\omega} \right)^2, \quad (75a)$$

$$e^{\beta(r)} = \frac{1 + 6 \left(\frac{M}{\omega} + \frac{\tilde{Q}^2}{\omega^2} \right)}{1 - \frac{2M}{r} + \frac{\tilde{Q}^2}{r^2} + \frac{2(\omega^2 + 3M\omega + 2\tilde{Q}^2)}{\omega^2} \frac{r}{\omega} + \frac{4M + \omega}{\omega} \left(\frac{r}{\omega} \right)^2}. \quad (75b)$$

The curvature scalar takes the form

$$\bar{R} = \frac{36\tilde{Q}^2}{(\omega^2 + 6M\omega + 6\tilde{Q}^2)(r + \omega)^2}. \quad (76)$$

It is easy to see that when considering the limit $\tilde{Q} \rightarrow 0$, the curvature scalar $\bar{R} \rightarrow 0$ and the solution (75) converge to a Schwarzschild-like solution (30).

Analyzing, globally, the curvature scalar (76) is positive for all r and it decreases with distance from the black hole. The maximum value occurs when $r_{\max} = 0$, taking the value

$\bar{R}_{\max} = \frac{36\tilde{Q}^2}{\omega^2(\omega^2+6M\omega+6\tilde{Q}^2)}$. In Figure 15, we represent the global behavior of the scalar curvature as a function of the distance, considering a specific case, where the point at which the external event horizon occurs is represented.

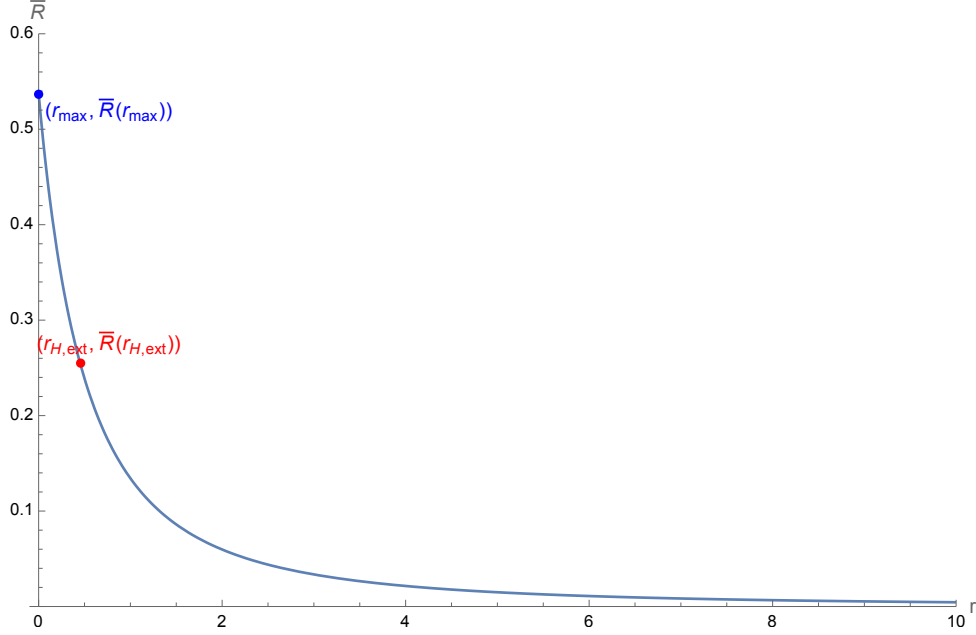


Figure 15: Global behavior of the scalar curvature \bar{R} as a function of the distance, assuming $M = 10$, $\omega = 1$, and $\tilde{Q} = 1$.

The Ricci scalar takes the form

$$R = -\frac{12\left((4M + \omega)r^2 + (\omega^2 + 3M\omega + 2\tilde{Q}^2)r - (\tilde{Q}^2 + M\omega)\omega\right)}{r^2\omega(\omega^2 + 6M\omega + 2\tilde{Q}^2)}. \quad (77)$$

It is easy to see that when considering the limit $\tilde{Q} \rightarrow 0$, the Ricci scalar R converges to a Schwarzschild-like solution (31). In Figure 16, we represent the global behavior of the scalar curvature as a function of the distance, considering a specific case, where the point at which the external event horizon occurs is represented.

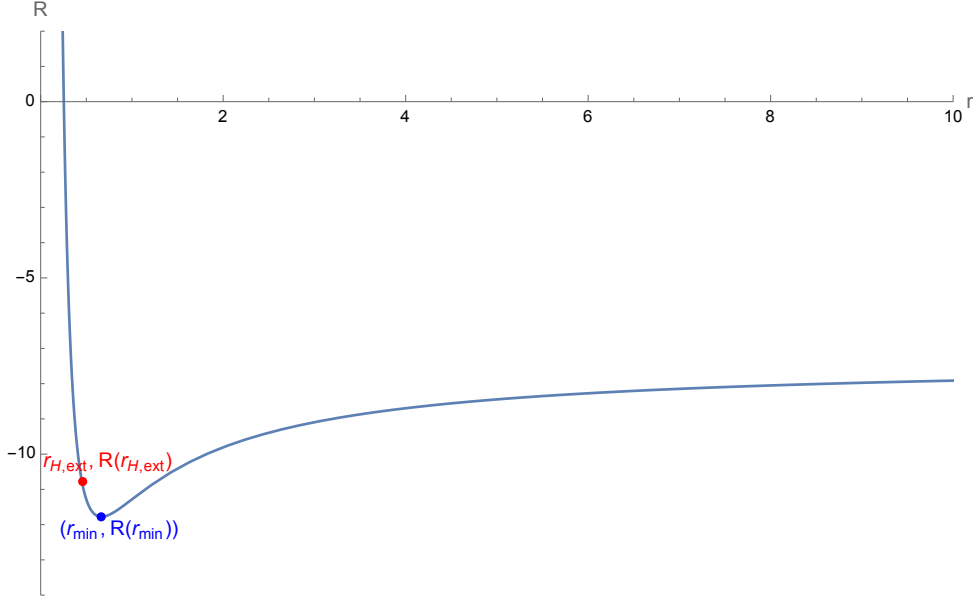


Figure 16: Global behavior of the standard Ricci scalar (built from the Levi–Civita part of the connection) as a function of the distance, assuming $M = 10$, $\omega = 1$, and $\tilde{Q} = 1$.

Analyzing, globally, the Ricci scalar (77), it is possible to see that when $r \rightarrow 0$, the Ricci scalar goes to infinity, $R \rightarrow +\infty$. When $r \rightarrow \infty$, the Ricci scalar converges to a non-null constant, $R \rightarrow -\frac{12(\omega+4M)}{\omega(\omega^2+6M\omega+6\tilde{Q}^2)}$. We can also note that the minimum value of Ricci scalar occurs when $r_{\min} = \frac{2\omega(\tilde{Q}^2+M\omega)}{\omega^2+3M\omega+2\tilde{Q}^2}$ and takes the value $R_{\min} = -\frac{3(4\tilde{Q}^2(\tilde{Q}^2+7M\omega+2\omega^2)+\omega^2(5M+\omega)^2)}{\omega^2(\tilde{Q}^2+M\omega)(\omega^2+6M\omega+6\tilde{Q}^2)}$.

In order to assess the nature of the singularities in this result, we compute the Kretschmann invariant. Thus, for this case, we obtain

$$K = \frac{h(r)}{r^8(r+w)^4(6Q^2+w(6M+w))^2}, \quad (78)$$

where $h(r)$ is a large polynomial expression of degree 8, which we opt to not display as it is not relevant for this analysis. It is possible to see that the Kretschmann invariant only diverges when $r = 0$ for any $M > 0$ and $\omega > 0$. Therefore, $r = 0$ is an essential singularity in the center of the black hole.

Due to the complexity of the solution obtained, it is not possible to provide a generic and complete analysis. We know that, under certain circumstances, we are in the presence of one or two event horizons, but it is difficult to rigorously define these values.

Tables 3, 4, and 5 represent the estimated values for the internal, $r_{H,\text{int}}$, and external, $r_{H,\text{ext}}$, event horizon considering the mass values 10^{-2} , 1, and 10^2 , respectively. We can conclude that, for the cases where there are event horizons which correspond to lower values for the effective charge, provided the Weyl constant is above a certain lower limit, the values of both horizons are strikingly similar.

\tilde{Q}	ω	$r_{H,\text{int}}$	$r_{H,\text{ext}}$
10^{-4}	10^{-7}	no $r_{H,\text{int}}$	no $r_{H,\text{ext}}$
	10^{-6}	no $r_{H,\text{int}}$	no $r_{H,\text{ext}}$
	10^{-5}	5.0425×10^{-7}	4.6474×10^{-6}
	10^{-4}	5.0005×10^{-7}	4.9541×10^{-5}
	10^{-3}	5.0001×10^{-7}	4.8747×10^{-4}
	10^{-2}	5.0001×10^{-7}	3.9997×10^{-3}
	10^{-1}	5.0001×10^{-7}	1.4285×10^{-2}
	10^1	5.0001×10^{-7}	1.9920×10^{-2}
	10^2	5.0001×10^{-7}	1.9992×10^{-2}
10^{-3}	10^{-5}	no $r_{H,\text{int}}$	no $r_{H,\text{ext}}$
	10^{-4}	no $r_{H,\text{int}}$	no $r_{H,\text{ext}}$
	10^{-3}	5.0568×10^{-5}	4.5281×10^{-4}
	10^{-2}	5.0131×10^{-5}	3.9677×10^{-3}
	10^{-1}	5.0126×10^{-5}	1.4247×10^{-2}
	10^0	5.0126×10^{-5}	1.9183×10^{-2}
	10^1	5.0126×10^{-5}	1.9870×10^{-2}
	10^3	5.0126×10^{-5}	1.9949×10^{-2}
10^5	5.0126×10^{-5}	1.9950×10^{-2}	
10^{-2}	for all $w > 0$	no $r_{H,\text{int}}$	no $r_{H,\text{ext}}$
10^{-1}	for all $w > 0$	no $r_{H,\text{int}}$	no $r_{H,\text{ext}}$
1	for all $w > 0$	no $r_{H,\text{int}}$	no $r_{H,\text{ext}}$
10^1	for all $w > 0$	no $r_{H,\text{int}}$	no $r_{H,\text{ext}}$
10^2	for all $w > 0$	no $r_{H,\text{int}}$	no $r_{H,\text{ext}}$
10^3	for all $w > 0$	no $r_{H,\text{int}}$	no $r_{H,\text{ext}}$
10^4	for all $w > 0$	no $r_{H,\text{int}}$	no $r_{H,\text{ext}}$

Table 3: Estimated values for the internal, $r_{H,\text{int}}$, and external, $r_{H,\text{ext}}$, event horizon considering the mass value $M = 10^{-2}$ and different values for the charge and the Weyl parameters, \tilde{Q} and ω , respectively.

\tilde{Q}	ω	$r_{H,int}$	$r_{H,ext}$
10^{-4}	10^{-9}	no $r_{H,int}$	no $r_{H,ext}$
	10^{-8}	no $r_{H,int}$	no $r_{H,ext}$
	10^{-7}	5.0423×10^{-9}	4.6487×10^{-8}
	10^{-6}	5.0004×10^{-9}	4.9665×10^{-7}
	10^{-5}	5.0000×10^{-9}	4.9967×10^{-6}
	10^{-4}	5.0000×10^{-9}	4.9995×10^{-5}
	10^{-3}	5.0000×10^{-9}	4.9987×10^{-4}
	10^{-2}	5.0000×10^{-9}	4.9875×10^{-3}
	10^{-1}	5.0000×10^{-9}	4.8780×10^{-2}
	1	5.0000×10^{-9}	4.0000×10^{-1}
	10^1	5.0000×10^{-9}	1.4286×10^0
	10^2	5.0000×10^{-9}	1.9231×10^0
	10^4	5.0000×10^{-9}	1.9992×10^0
	10^{-3}	10^{-7}	no $r_{H,int}$
10^{-6}		no $r_{H,int}$	no $r_{H,ext}$
10^{-5}		5.0423×10^{-7}	4.6487×10^{-6}
10^{-4}		5.0004×10^{-7}	4.9664×10^{-5}
10^{-3}		5.0000×10^{-7}	4.9954×10^{-4}
10^{-2}		5.0000×10^{-7}	4.9872×10^{-3}
10^{-1}		5.0000×10^{-7}	4.8780×10^{-2}
1		5.0000×10^{-7}	4.0000×10^{-1}
10^1		5.0000×10^{-7}	1.4286×10^0
10^{-2}	10^{-5}	no $r_{H,int}$	no $r_{H,ext}$
	10^{-4}	no $r_{H,int}$	no $r_{H,ext}$
	10^{-3}	5.0425×10^{-5}	4.6474×10^{-4}
	10^{-2}	5.0005×10^{-5}	4.9541×10^{-3}
	10^{-1}	5.0001×10^{-5}	4.8747×10^{-2}
	1	5.0001×10^{-5}	3.9997×10^{-1}
	10^1	5.0001×10^{-5}	1.4285×10^0
	10^2	5.0001×10^{-5}	1.9230×10^0
	10^3	5.0001×10^{-5}	1.9920×10^0
10^{-1}	10^{-3}	no $r_{H,int}$	no $r_{H,ext}$
	10^{-2}	no $r_{H,int}$	no $r_{H,ext}$
	10^{-1}	5.0568×10^{-3}	4.5281×10^{-2}
	1	5.0131×10^{-3}	3.9677×10^{-1}
	10^1	5.0126×10^{-3}	1.4247×10^0
	10^2	5.0126×10^{-3}	1.9183×10^0
	10^3	5.0126×10^{-3}	1.9870×10^0
	10^4	5.0126×10^{-3}	1.9942×10^0
	10^5	5.0126×10^{-3}	1.9949×10^0
1	for all $w > 0$	no $r_{H,int}$	no $r_{H,ext}$
10^1	for all $w > 0$	no $r_{H,int}$	no $r_{H,ext}$
10^2	for all $w > 0$	no $r_{H,int}$	no $r_{H,ext}$
10^3	for all $w > 0$	no $r_{H,int}$	no $r_{H,ext}$
10^4	for all $w > 0$	no $r_{H,int}$	no $r_{H,ext}$

Table 4: Estimated values for the internal, $r_{H,int}$, and external, $r_{H,ext}$, event horizon considering the mass value $M = 1$ and different values for the charge and the Weyl parameters, \tilde{Q} and ω , respectively.

Since the analytical solutions are too cumbersome to be treated in the derivation of the corresponding thermodynamical quantities, this analysis will not be pursued for the Reissner–Nordström case.

\tilde{Q}	ω	$r_{H,int}$	$r_{H,ext}$	
10^{-4}	10^{-11}	no $r_{H,int}$	no $r_{H,ext}$	
	10^{-10}	no $r_{H,int}$	no $r_{H,ext}$	
	10^{-9}	5.0423×10^{-11}	4.6487×10^{-10}	
	10^{-8}	5.0004×10^{-11}	4.9665×10^{-9}	
	10^{-7}	5.0000×10^{-11}	4.9967×10^{-8}	
	10^{-6}	5.0000×10^{-11}	4.9997×10^{-7}	
	10^{-4}	5.0000×10^{-11}	5.0000×10^{-5}	
	10^{-2}	5.0000×10^{-11}	4.9999×10^{-3}	
	1	5.0000×10^{-11}	4.9875×10^{-1}	
	10^1	5.0000×10^{-11}	4.8780×10^0	
	10^2	5.0000×10^{-11}	4.0000×10^1	
	10^3	5.0000×10^{-11}	1.4286×10^2	
	10^4	5.0000×10^{-11}	1.9231×10^2	
	10^6	5.0000×10^{-11}	1.9992×10^2	
10^{-3}	10^{-9}	no $r_{H,int}$	no $r_{H,ext}$	
	10^{-8}	no $r_{H,int}$	no $r_{H,ext}$	
	10^{-7}	5.0423×10^{-9}	4.6487×10^{-8}	
	10^{-6}	5.0004×10^{-9}	4.9665×10^{-7}	
	10^{-5}	5.0000×10^{-9}	4.9967×10^{-6}	
	10^{-4}	5.0000×10^{-9}	4.9997×10^{-5}	
	10^{-3}	5.0000×10^{-9}	5.0000×10^{-4}	
	10^{-2}	5.0000×10^{-9}	4.9999×10^{-3}	
	10^{-1}	5.0000×10^{-9}	4.9987×10^{-2}	
	1	5.0000×10^{-9}	4.9875×10^{-1}	
	10^1	5.0000×10^{-9}	4.8780×10^0	
	10^2	5.0000×10^{-9}	4.0000×10^1	
	10^3	5.0000×10^{-9}	1.4286×10^2	
	10^5	5.0000×10^{-9}	1.9920×10^2	
10^{-2}	10^{-7}	no $r_{H,int}$	no $r_{H,ext}$	
	10^{-6}	no $r_{H,int}$	no $r_{H,ext}$	
	10^{-5}	5.0423×10^{-7}	4.6487×10^{-6}	
	10^{-4}	5.0004×10^{-7}	4.9665×10^{-5}	
	10^{-3}	5.0000×10^{-7}	4.9967×10^{-4}	
	10^{-2}	5.0000×10^{-7}	4.9995×10^{-3}	
	10^{-1}	5.0000×10^{-7}	4.9987×10^{-2}	
	1	5.0000×10^{-7}	4.9875×10^{-1}	
	10^1	5.0000×10^{-7}	4.8780×10^0	
	10^2	5.0000×10^{-7}	4.0000×10^1	
	10^3	5.0000×10^{-7}	1.4286×10^2	
	10^6	5.0000×10^{-7}	1.9992×10^2	
	10^{-1}	for all $w > 0$	no $r_{H,int}$	no $r_{H,ext}$
	1	for all $w > 0$	no $r_{H,int}$	no $r_{H,ext}$
10^1	for all $w > 0$	no $r_{H,int}$	no $r_{H,ext}$	
10^2	for all $w > 0$	no $r_{H,int}$	no $r_{H,ext}$	
10^3	for all $w > 0$	no $r_{H,int}$	no $r_{H,ext}$	
10^4	for all $w > 0$	no $r_{H,int}$	no $r_{H,ext}$	

Table 5: Estimated values for the internal, $r_{H,int}$, and external, $r_{H,ext}$, event horizon considering the mass value $M = 10^2$ and different values for the charge and the Weyl parameters, \tilde{Q} and ω , respectively.

5 Conclusions

In this work, we analyzed black hole solutions of a non-minimally coupled Weyl connection gravity in the form of generalized Schwarzschild and Reissner–Nordstrøm solutions both in a vacuum and in the presence of matter fluids behaving as a cosmological constant. The Weyl connection is a particular case of non-metricity, and, in the context of these alternative theories of gravity, leads to black hole solutions for which the scalar curvature is non-vanishing.

When in a vacuum, the model under study is equivalent to $f(R)$ theories with the Weyl connection. Thus, in comparison with constant curvature solutions for vacuum metric $f(R)$ theories, our model introduces a term linear to the radius, r , and a corrected cosmological constant in the solutions for the metric functions for Schwarzschild-like black holes. In addition, no solutions of the Reissner–Nordstrøm form are found.

However, the non-minimally coupled Weyl connection gravity model for non-vacuum solutions behaves differently. In particular, matter fields of the form of a cosmological constant lead to Schwarzschild-like black holes exhibiting a behavior analogous to the vacuum case with a contribution also arising from this matter Lagrangian choice. This is mathematically equivalent to a reparametrization of vacuum $f(R)$ theories; however, physically, they are different because one is assuming a contribution from vacuum energy or matter fields behaving as a cosmological constant that is different from an integration constant or a numerical rescaling of functions, in the same spirit of Ref. [40]. Moreover, Reissner–Nordstrøm solutions can be found with a linear term in r and corrected/dressed charge and cosmological constant in the solution for the metric functions.

There are several studies considering $f(R)$ theories that analyze black hole solutions. In Ref. [36], the authors present a Schwarzschild-like solution with an asymptotic behavior similar to ours; the universe expands with a r^2 factor. However, in our case, a linear contribution also appears. Additionally, in Ref. [35], it is possible to find, in $f(R)$ theory, a solution to a charged black hole in an expansive anti-de Sitter space with r^2 . Therefore, our Reissner–Nordstrøm solution presents the same asymptotic behavior; however, also with an additional linear term.

Similar to Ref. [41], where the authors provided numerical black hole solutions in the Weyl conformal geometry that also have an expansion behavior, our study found an exact solution that presents a Schwarzschild term inversely proportional to r and two more terms proportional to r and r^2 . Moreover, black hole solutions in 4D Einstein–Gauss–Bonnet theory exhibit, like ours, an asymptotically non-flat behavior given the r^2 factor in the metric solution [61].

In fact, our analysis shows that the $r = 0$ singularity is an essential one; thus, we are not able to remove it. Since the Kretschmann invariants for the cases we analyzed depend only on the radial coordinate and on constants, we cannot find a relation among the numerator components such that we could eliminate the exact dependency on r at the denominator. However, if we consider a Hayward metric ansatz, we may circumvent this issue, thus having a model lacking a central singularity. This leads to an entire new work in the future.

Other solutions of black holes can exist in this gravity model. In particular, Kerr solutions, even in the form of slowly-rotating spherically symmetric space–times or black hole solutions different from analytics ones from general relativity, may be obtained in future work, but they fall outside of the scope of the present paper. Moreover, the results found in this work may be relevant to discriminate between modified gravity theories, provided that numerical simulations allow the incorporation of extra degrees of freedom. In particular, the gravitational wave data from the collision of black holes may be an interesting avenue of study.

Acknowledgements

M. M. Lima acknowledges support from Fundo Regional da Ciência e Tecnologia and Azores Government through the Fellowship M3.1.a/F/001/2022.

A Generalized Riemann Curvature Tensor Components

In this section, we will enumerate the non-vanished generalized Riemann curvature tensor components given by (3). Note that the tensor is antisymmetric in the last two indices, $\bar{R}_{\mu\sigma\nu}^\rho = -\bar{R}_{\mu\nu\sigma}^\rho$. We will present only one of them.

A.1 First Ansatz: $A_\mu = (0, A(r), 0, 0)$

Considering (20) and the ansatz $A_\mu = (0, A(r), 0, 0)$, the non-vanishing components of the generalized Riemann curvature tensor are as follows:

$$R_{101}^0 = \frac{1}{4} (2A'(r) + (A(r) - \alpha'(r))(\alpha'(r) - \beta'(r)) - 2\alpha''(r)) \quad (79)$$

$$R_{220}^0 = \frac{1}{4} e^{-\beta(r)} r (-2 + rA(r))(A(r) - \alpha'(r)) \quad (80)$$

$$R_{330}^0 = \frac{1}{4} e^{-\beta(r)} r (-2 + rA(r))(A(r) - \alpha'(r)) \sin^2(\theta) \quad (81)$$

$$R_{001}^1 = \frac{1}{4} e^{\alpha(r)-\beta(r)} (2A'(r) + (A(r) - \alpha'(r))(\alpha'(r) - \beta'(r)) - 2\alpha''(r)) \quad (82)$$

$$R_{221}^1 = \frac{1}{4} e^{-\beta(r)} r (-2(A(r) + rA'(r)) + (-2 + rA(r))\beta'(r)) \quad (83)$$

$$R_{331}^1 = \frac{1}{4} e^{-\beta(r)} r (-2(A(r) + rA'(r)) + (-2 + rA(r))\beta'(r)) \sin^2(\theta) \quad (84)$$

$$R_{020}^2 = R_{030}^3 = \frac{1}{4r} e^{\alpha(r)-\beta(r)} (-2 + rA(r))(A(r) - \alpha'(r)) \quad (85)$$

$$R_{112}^2 = R_{113}^3 = \frac{1}{4r} (-2(A(r) + rA'(r)) + (-2 + rA(r))\beta'(r)) \quad (86)$$

$$R_{323}^2 = \frac{1}{4} (4 - e^{-\beta(r)}(-2 + rA(r))^2) \sin^2(\theta) \quad (87)$$

$$R_{232}^3 = 1 - \frac{1}{4} e^{-\beta(r)}(-2 + rA(r))^2 \quad (88)$$

A.2 Second Ansatz: $A_\mu = (A_0(r), A_1(r), 0, 0)$

Considering (20) and the ansatz $A_\mu = (A_0(r), A_1(r), 0, 0)$, the non-vanishing components of the generalized Riemann curvature tensor are as follows:

$$R_{001}^0 = R_{101}^1 = R_{201}^2 = R_{301}^3 = \frac{A_0'(r)}{2} \quad (89a)$$

$$R_{101}^0 = \frac{1}{4} (2A_1'(r) + (A_1(r) - \alpha'(r))(\alpha'(r) - \beta'(r)) - 2\alpha''(r)) \quad (89b)$$

$$R_{220}^0 = \frac{1}{4} e^{-\beta(r)} r (-2 + rA_1(r))(A_1(r) - \alpha'(r)) \quad (89c)$$

$$R_{221}^0 = \frac{1}{4} e^{-\alpha(r)} r^2 (2A_0'(r) + A_0(r)(A_1(r) - \alpha'(r))) \quad (89d)$$

$$R_{330}^0 = \frac{1}{4} e^{-\beta(r)} r (-2 + rA_1(r))(A_1(r) - \alpha'(r)) \sin^2(\theta) \quad (89e)$$

$$R_{331}^0 = \frac{1}{4} e^{-\alpha(r)} r^2 (2A_0'(r) + A_0(r)(A_1(r) - \alpha'(r))) \sin^2(\theta) \quad (89f)$$

$$R_{001}^1 = \frac{1}{4} e^{\alpha(r)-\beta(r)} (2A_1'(r) + (A_1(r) - \alpha'(r))(\alpha'(r) - \beta'(r)) - 2\alpha''(r)) \quad (89g)$$

$$R_{220}^1 = \frac{1}{4} e^{-\beta(r)} r^2 A_0(r) (-A_1(r) + \alpha'(r)) \quad (89h)$$

$$R_{221}^1 = \frac{1}{4} r \left(-e^{-\alpha(r)} r A_0(r)^2 + e^{-\beta(r)} (-2(A_1(r) + rA_1'(r)) + (-2 + rA_1(r))\beta'(r)) \right) \quad (89i)$$

$$R_{313}^1 = \frac{1}{4} r \left(e^{-\alpha(r)} r A_0(r)^2 + e^{-\beta(r)} (2(A_1(r) + rA_1'(r)) + (2 - rA_1(r))\beta'(r)) \right) \sin^2(\theta) \quad (89j)$$

$$R_{330}^1 = \frac{1}{4} e^{-\beta(r)} r^2 A_0(r) (-A_1(r) + \alpha'(r)) \sin^2(\theta) \quad (89k)$$

$$R_{020}^2 = R_{030}^3 = \frac{1}{4r} e^{\alpha(r)-\beta(r)} (-2 + rA_1(r))(A_1(r) - \alpha'(r)) \quad (89l)$$

$$R_{021}^2 = R_{031}^3 = \frac{1}{4} (2A_0'(r) + A_0(r)(A_1(r) - \alpha'(r))) \quad (89m)$$

$$R_{102}^2 = R_{103}^3 = \frac{1}{4} A_0(r) (-A_1(r) + \alpha'(r)) \quad (89n)$$

$$R_{121}^2 = R_{131}^3 = \frac{1}{4r} e^{-\alpha(r)+\beta(r)} r A_0(r)^2 + 2(rA_1'(r) + \beta'(r)) + A_1(r)(2 - r\beta'(r)) \quad (89o)$$

$$R_{232}^3 = \frac{1}{4} \left(4 - e^{-\beta(r)} (-2 + rA_1(r))^2 + e^{-\alpha(r)} r^2 A_0(r)^2 \right) \quad (89p)$$

$$R_{323}^2 = \frac{1}{4} \left(4 - e^{-\beta(r)} (-2 + rA_1(r))^2 + e^{-\alpha(r)} r^2 A_0(r)^2 \right) \sin^2(\theta) \quad (89q)$$

References

- [1] Capozziello, S.; De Laurentis, M. Extended Theories of Gravity. *Phys. Rep.* **2011**, *509*, 167–321. <https://doi.org/https://doi.org/10.1016/j.physrep.2011.09.003>.
- [2] Nojiri, S.; Odintsov, S.D. Unified cosmic history in modified gravity: From $F(R)$ theory to Lorentz non-invariant models. *Phys. Rep.* **2011**, *505*, 59–144. <https://doi.org/10.1016/j.physrep.2011.04.001>.
- [3] Nojiri, S.; Odintsov, S.; Oikonomou, V. Modified gravity theories on a nutshell: Inflation, bounce and late-time evolution. *Phys. Rep.* **2017**, *692*, 1–104. <https://doi.org/10.1016/j.physrep.2017.06.001>.

- [4] Sotiriou, T.P.; Faraoni, V. $f(R)$ theories of gravity. *Rev. Mod. Phys.* **2010**, *82*, 451–497. <https://doi.org/10.1103/RevModPhys.82.451>.
- [5] De Felice, A.; Tsujikawa, S. $f(R)$ Theories. *Living Rev. Relativ.* **2010**, *13*, 3. <https://doi.org/10.12942/lrr-2010-3>.
- [6] Bertolami, O.; Böhmer, C.G.; Harko, T.; Lobo, F.S.N. Extra force in $f(R)$ modified theories of gravity. *Phys. Rev. D* **2007**, *75*, 104016. <https://doi.org/10.1103/PhysRevD.75.104016>.
- [7] Bertolami, O.; Páramos, J. Mimicking dark matter through a non-minimal gravitational coupling with matter. *J. Cosmol. Astropart. Phys.* **2010**, *03*, 009. <https://doi.org/10.1088/1475-7516/2010/03/009>.
- [8] Bertolami, O.; Frazão, P.; Páramos, J. Mimicking dark matter in galaxy clusters through a nonminimal gravitational coupling with matter. *Phys. Rev. D* **2012**, *86*, 044034. <https://doi.org/10.1103/PhysRevD.86.044034>.
- [9] Bertolami, O.; Frazão, P.; Páramos, J. Accelerated expansion from a nonminimal gravitational coupling to matter. *Phys. Rev. D* **2010**, *81*, 104046. <https://doi.org/10.1103/PhysRevD.81.104046>.
- [10] Bertolami, O.; Gomes, C. The Layzer-Irvine equation in theories with non-minimal coupling between matter and curvature. *J. Cosmol. Astropart. Phys.* **2014**, *09*, 010. <https://doi.org/10.1088/1475-7516/2014/09/010>.
- [11] Olmo, G.J.; Rubiera-Garcia, D. Brane-world and loop cosmology from a gravity–matter coupling perspective. *Phys. Lett. B* **2015**, *740*, 73–79. <https://doi.org/10.1016/j.physletb.2014.11.034>.
- [12] Gomes, C.; Rosa, J.; Bertolami, O. Inflation in non-minimal matter-curvature coupling theories. *J. Cosmol. Astropart. Phys.* **2017**, *06*, 021. <https://doi.org/10.1088/1475-7516/2017/06/021>.
- [13] Bertolami, O.; Gomes, C.; Lobo, F.S.N. Gravitational waves in theories with a non-minimal curvature-matter coupling. *Eur. Phys. J. C* **2018**, *78*, 303. <https://doi.org/10.1140/epjc/s10052-018-5781-5>.
- [14] Ferreira, T.D.; Silva, N.A.; Bertolami, O.; Gomes, C.; Guerreiro, A. Simulating N-body systems for alternative theories of gravity using solvers from nonlocal optics. In Proceedings of the Fourth International Conference on Applications of Optics and Photonics, Lisbon, Portugal, 31 May–4 June 2019; Costa, M.F.P.C.M.M., Ed.; SPIE: Bellingham, WA USA, 2019; Volume 11207, p. 1120710. <https://doi.org/10.1117/12.2527295>.
- [15] Ferreira, T.D.; Silva, N.A.; Bertolami, O.; Gomes, C.; Guerreiro, A. Using numerical methods from nonlocal optics to simulate the dynamics of N-body systems in alternative theories of gravity. *Phys. Rev. E* **2020**, *101*, 023301. <https://doi.org/10.1103/PhysRevE.101.023301>.
- [16] Bertolami, O.; Gomes, C. Nonminimally coupled Boltzmann equation: Foundations. *Phys. Rev. D* **2020**, *102*, 084051. <https://doi.org/10.1103/PhysRevD.102.084051>.
- [17] Gomes, C. Jeans instability in non-minimal matter-curvature coupling gravity. *Eur. Phys. J. C* **2020**, *80*, 633. <https://doi.org/10.1140/epjc/s10052-020-8189-y>.

- [18] Gomes, C.; Ourabah, K. Quantum kinetic theory of Jeans instability in non-minimal matter-curvature coupling gravity. *Eur. Phys. J. C* **2023**, *83*, 40. <https://doi.org/10.1140/epjc/s10052-023-11184-9>.
- [19] March, R.; Bertolami, O.; Muccino, M.; Gomes, C.; Dell’Agnello, S. Cassini and extra force constraints to nonminimally coupled gravity with a screening mechanism. *Phys. Rev. D* **2022**, *105*, 044048. <https://doi.org/10.1103/PhysRevD.105.044048>.
- [20] Bertolami, O.; Lima, M.M.; Mena, F.C. Primordial magnetic fields in theories of gravity with non-minimal coupling between curvature and matter. *Gen. Rel. Grav.* **2022**, *54*, 82. <https://doi.org/10.1007/s10714-022-02968-7>.
- [21] Bertolami, O.; Gomes, C.; Sá, P.M. Theories of gravity with nonminimal matter-curvature coupling and the de Sitter swampland conjectures. *Phys. Rev. D* **2023**, *107*, 084009. <https://doi.org/10.1103/PhysRevD.107.084009>.
- [22] Beltrán Jiménez, J.; Heisenberg, L.; Koivisto, T.S. The Geometrical Trinity of Gravity. *Universe* **2019**, *5*, 173. <https://doi.org/10.3390/universe5070173>.
- [23] Linder, E.V. Einstein’s other gravity and the acceleration of the Universe. *Phys. Rev. D* **2010**, *81*, 127301; Erratum in *Phys. Rev. D* **2010**, *82*, 109902. <https://doi.org/10.1103/PhysRevD.81.127301>.
- [24] Jiménez, J.B.; Heisenberg, L.; Koivisto, T. Coincident general relativity. *Phys. Rev. D* **2018**, *98*, 044048. <https://doi.org/10.1103/PhysRevD.98.044048>.
- [25] Heisenberg, L. Review on $f(Q)$ gravity. *Phys. Rep.* **2024**, *1066*, 1–78. <https://doi.org/10.1016/j.physrep.2024.02.001>.
- [26] Harko, T.; Koivisto, T.S.; Lobo, F.S.N.; Olmo, G.J.; Rubiera-Garcia, D. Coupling matter in modified Q gravity. *Phys. Rev. D* **2018**, *98*, 084043. <https://doi.org/10.1103/PhysRevD.98.084043>.
- [27] Kaluza, T. Zum Unitätsproblem in der Physik. *K. Preuss. Akad. Wiss* **1921**, *1*, 966.
- [28] Klein, O. Quantentheorie und fünfdimensionale Relativitätstheorie. *Z. Phys.* **1926**, *37*, 895–906.
- [29] Cheng, H. Possible Existence of Weyl’s Vector Meson. *Phys. Rev. Lett.* **1988**, *61*, 2182–2184. <https://doi.org/10.1103/PhysRevLett.61.2182>.
- [30] Aringazin, A.K.; Mikhailov, A.L. Matter fields in spacetime with vector nonmetricity. *Class. Quantum Gravity* **1991**, *8*, 1685. <https://doi.org/10.1088/0264-9381/8/9/004>.
- [31] Ne’eman, Y.; Hehl, F.W. Test matter in a spacetime with nonmetricity. *Class. Quantum Gravity* **1997**, *14*, A251. <https://doi.org/10.1088/0264-9381/14/1A/020>.
- [32] Gomes, C.; Bertolami, O. Nonminimally coupled Weyl gravity. *Class. Quantum Gravity* **2019**, *36*, 235016. <https://doi.org/10.1088/1361-6382/ab52b9>.
- [33] Baptista, R.; Bertolami, O. Cosmological solutions of the non-minimally coupled Weyl connection gravity theories. *Class. Quantum Gravity* **2020**, *37*, 085011. <https://doi.org/10.1088/1361-6382/ab7bb8>.
- [34] Baptista, R.; Bertolami, O. An Ostrogradsky instability analysis of non-minimally coupled Weyl connection gravity theories. *Gen. Relativ. Gravit.* **2021**, *53*. <https://doi.org/10.1007/s10714-021-02784-58>.

- [35] de la Cruz-Dombriz, A.; Dobado, A.; Maroto, A.L. Black holes in $f(R)$ theories. *Phys. Rev. D* **2009**, *80*, 124011. <https://doi.org/10.1103/PhysRevD.80.124011>.
- [36] Capozziello, S.; Laurentis, M.D.; Stabile, A. Axially symmetric solutions in $f(R)$ -gravity. *Class. Quantum Gravity* **2010**, *27*, 165008. <https://doi.org/10.1088/0264-9381/27/16/165008>.
- [37] Moon, T.; Myung, Y.S.; Son, E.J. $f(R)$ black holes. *Gen. Relativ. Gravit.* **2011**, *43*, 3079–3098. <https://doi.org/10.1007/s10714-011-1225-3>.
- [38] Rostami, M.; Sadeghi, J.; Miraboutalebi, S. The static black hole in $f(R)$ gravity with thermal corrections and phase transition. *Phys. Dark Universe* **2020**, *29*, 100590. <https://doi.org/10.1016/j.dark.2020.100590>.
- [39] Nashed, G.G.L.; Capozziello, S. Charged spherically symmetric black holes in $f(R)$ gravity and their stability analysis. *Phys. Rev. D* **2019**, *99*, 104018. <https://doi.org/10.1103/PhysRevD.99.104018>.
- [40] Bertolami, O.; Cadoni, M.; Porru, A. Black hole solutions of gravity theories with non-minimal coupling between matter and curvature. *Class. Quantum Gravity* **2015**, *32*, 205009. <https://doi.org/10.1088/0264-9381/32/20/205009>.
- [41] Yang, J.-Z.; Shahidi, S.; Harko, T. Black hole solutions in the quadratic Weyl conformal geometric theory of gravity. *Eur. Phys. J. C* **2022**, *82*, 1171. <https://doi.org/10.1140/epjc/s10052-022-11131-0>.
- [42] Momennia, M.; Hendi, S. Quasinormal modes of black holes in Weyl gravity: Electromagnetic and gravitational perturbations. *Eur. Phys. J. C* **2020**, *80*, 505. <https://doi.org/10.1140/epjc/s10052-020-8051-2>.
- [43] Wald, R. The Thermodynamics of Black Holes. *Living Rev. Rel.* **2001**, *4*, 6. <https://doi.org/10.12942/lrr-2001-6>.
- [44] Heisenberg, L.; Kase, R.; Minamitsuji, M.; Tsujikawa, S. Black holes in vector-tensor theories. *J. Cosmol. Astropart. Phys.* **2017**, *08*, 024. <https://doi.org/10.1088/1475-7516/2017/08/024>.
- [45] Fan, Z.Y. Black holes in vector-tensor theories and their thermodynamics. *Eur. Phys. J. C* **2018**, *78*, 65. <https://doi.org/10.1140/epjc/s10052-018-5540-7>.
- [46] Mureika, J.R.; Moffat, J.W.; Faizal, M. Black hole thermodynamics in MODified Gravity (MOG). *Phys. Lett. B* **2016**, *757*, 528–536. <https://doi.org/10.1016/j.physletb.2016.04.041>.
- [47] Ghaderi, K.; Malakolkalami, B. Thermodynamics of the Schwarzschild and the Reissner–Nordström black holes with quintessence. *Nucl. Phys. B* **2016**, *903*, 10–18. <https://doi.org/10.1016/j.nuclphysb.2015.11.019>.
- [48] Gomes, D.; Maluf, R.; Almeida, C. Thermodynamics of Schwarzschild-like black holes in modified gravity models. *Ann. Phys.* **2020**, *418*, 168198. <https://doi.org/10.1016/j.aop.2020.168198>.
- [49] Sebastiani, L.; Zerbini, S. Static spherically symmetric solutions in $F(R)$ gravity. *Eur. Phys. J. C* **2011**, *71*, 1591. <https://doi.org/10.1140/epjc/s10052-011-1591-8>.

- [50] Brown, J.D. Action functionals for relativistic perfect fluids. *Class. Quantum Gravity* **1993**, *10*, 1579. <https://doi.org/10.1088/0264-9381/10/8/017>.
- [51] Bertolami, O.; Lobo, F.S.N.; Páramos, J. Nonminimal coupling of perfect fluids to curvature. *Phys. Rev. D* **2008**, *78*, 064036. <https://doi.org/10.1103/PhysRevD.78.064036>.
- [52] Henry, R.C. Kretschmann Scalar for a Kerr-Newman Black Hole. *Astrophys. J.* **2000**, *535*, 350. <https://doi.org/10.1086/308819>.
- [53] Campista, M.; Chan, R.; da Silva, M.; Goldoni, O.; Satheeshkumar, V.; Villas da Rocha, J.F. Vacuum solutions in the Einstein–Aether Theory. *Can. J. Phys.* **2020**, *98*, 917–928. <https://doi.org/10.1139/cjp-2019-0321>.
- [54] Chan, R.; Silva, M.; Satheeshkumar, V. Spherically symmetric analytic solutions and naked singularities in Einstein–Aether theory. *Eur. Phys. J. C* **2021**, *81*, 317. <https://doi.org/10.1140/epjc/s10052-021-09120-w>.
- [55] Capozziello, S.; De Bianchi, S.; Battista, E. Avoiding singularities in Lorentzian-Euclidean black holes: The role of atemporality. *Phys. Rev. D* **2024**, *109*, 104060. <https://doi.org/10.1103/PhysRevD.109.104060>.
- [56] Nashed, G. Extension of Hayward black hole in $f(R)$ gravity coupled with a scalar field. *Phys. Dark Universe* **2024**, *44*, 101462. <https://doi.org/10.1016/j.dark.2024.101462>.
- [57] Yang, J.Z.; Shahidi, S.; Harko, T.; Liang, S.D. Black hole solutions in modified gravity induced by quantum metric fluctuations. *Phys. Dark Universe* **2021**, *31*, 100756. <https://doi.org/10.1016/j.dark.2020.100756>.
- [58] Shankaranarayanan, S. Temperature and entropy of Schwarzschild–de Sitter space-time. *Phys. Rev. D* **2003**, *67*, 084026. <https://doi.org/10.1103/PhysRevD.67.084026>.
- [59] Ma, M.S.; Zhao, R. Corrected form of the first law of thermodynamics for regular black holes. *Class. Quantum Gravity* **2014**, *31*, 245014. <https://doi.org/10.1088/0264-9381/31/24/245014>.
- [60] Maluf, R.V.; Neves, J.C.S. Thermodynamics of a class of regular black holes with a generalized uncertainty principle. *Phys. Rev. D* **2018**, *97*, 104015. <https://doi.org/10.1103/PhysRevD.97.104015>.
- [61] Glavan, D.; Lin, C. Einstein-Gauss-Bonnet Gravity in Four-Dimensional Spacetime. *Phys. Rev. Lett.* **2020**, *124*, 081301. <https://doi.org/10.1103/PhysRevLett.124.081301>.